Journal Pre-proof

S.L.C. Giering, R. Sanders, S. Blackbird, N. Briggs, F. Carvalho, H. East, B. Espinola, S.A. Henson, K. Kiriakoulakis, M.H. Iversen, R.S. Lampitt, K. Pabortsava, C. Pebody, K. Peele, C. Preece, K. Saw, M. Villa-Alfageme, G.A. Wolff

This is a PDF file of an article that has undergone enhancements after acceptance, such as the addition of a cover page and metadata, and formatting for readability, but it is not yet the definitive version of record. This version will undergo additional copyediting, typesetting and review before it is published in its final form, but we are providing this version to give early visibility of the article. Please note that, during the production process, errors may be discovered which could affect the content, and all legal disclaimers that apply to the journal pertain.

Author statement

Giering: Conceptualization, Methodology, Formal analysis, Investigation, Validation, Visualization, Writing

Sanders: Conceptualization, Funding acquisition, Investigation, Writing,

Blackbird: Sample analysis

Briggs: Methodology, Investigation, Validation, Writing

Carvalho: Methodology, Investigation, Validation, Writing

East: Sample analysis, Data curation, Investigation

Espinola: Sample analysis, Investigation

Henson: Conceptualization, Writing

Kiriakoulakis: Sample collection

Iversen: Sample collection, Writing

Lampitt: Conceptualization, Sample collection

Pabortsava: Sample analysis

Pebody: Sample analysis

Peele: Sample analysis

Preece: Sample analysis

Saw: Engineering, Methodology

Villa-Alfageme: Investigation, Writing

Wolff: Investigation, Writing

Vertical imbalance in organic carbon budgets is indicative of a missing vertical transfer during a phytoplankton bloom near South Georgia (COMICS)

Giering SLC[1], R Sanders[1], S Blackbird[2], N Briggs[1], F Carvalho[1], H East[1], B Espinola[1], SA Henson[1], K Kiriakoulakis[3], MH Iversen[4,5], RS Lampitt[1], K Pabortsava[1], C Pebody[1], K Peele[1], C Preece[2], K Saw[1], M Villa-Alfageme[6], GA Wolff[2]

[1]National Oceanography Centre, Southampton, SO14 3ZH, UK

[2]School of Environmental Sciences, University of Liverpool, Liverpool, L69 3GP, UK

[3]School of Biological and Environmental Sciences, Liverpool John Moores University, Liverpool, L3 3AF, UK

[4]Alfred Wegener Institute for Polar and Marine Research, Bremerhaven, 28570, Germany

[5]MARUM and University of Bremen, Bremen, 28359, Germany

[6]Dept. of Applied Physics II. ETSIE. universidad de Sevilla, Sevilla, 41012, Spain

Abstract

The biological carbon pump, driven principally by surface production and sinking of organic matter to deep water and its subsequent remineralisation to CO_2 maintains atmospheric CO_2 around 200 ppm lower than it would be if the ocean were abiotic. One important driver of the magnitude of this effect is the depth to which organic matter sinks before it is remineralised, a parameter we have limited confidence in measuring given the difficulty involved in balancing sources and sinks in the ocean's interior. This imbalance is due, in part, to our inability to measure respiration directly and our reliance on radiotracer-based proxies. One solution to these problems might be a temporal offset in which organic carbon accumulates in the mesopelagic zone (100 - 1000 m depth) early in the productive season prior to it being consumed later, a situation which could lead to a net apparent sink occurring if a steady state assumption is applied as is often the approach. In this work, we develop a novel accounting method to address this issue, independent of respiration measurements, by estimating fluxes into and accumulation within distinct vertical layers in the mesopelagic. We apply this approach to a time series of measurements of particle sinking velocities and interior organic carbon concentrations made during the declining phase of a large diatom bloom in a low-circulation region of the Southern Ocean downstream of South Georgia. Our data show that the major export event led to a significant accumulation of organic matter in the upper mesopelagic (100-200 m depth) which declined over several weeks, implying that temporal offsets need to be considered when compiling budgets. However, even when accounting for this accumulation, a mismatch in the vertically resolved organic carbon budget remained, implying that there are likely widespread processes that we do not yet understand that redistribute material vertically in the mesopelagic.

Keywords
Biological Carbon Pump, sinking particles, mesopelagic carbon budget, Southern Ocean

1 | Introduction

41   Biological processes in the ocean play an important role in the global carbon cycle, exporting
42   carbon from the ocean surface to the deep ocean, where it can be stored over long time scales.
43   Without this process, called the 'biological carbon pump' (Giering and Humphreys, 2018; Volk
44   and Hoffert, 1985), atmospheric CO_2 concentrations would be, according to models, 200 ppm
45   higher than at present (Parekh et al., 2006). A key driver of the biological carbon pump is the
46   formation of carbon-rich sinking particles, such as aggregated phytoplankton and detritus or
47   faecal pellets, and their transport to the deep ocean, where they remain out of contact with the
48   atmosphere. In the deep ocean, sinking particles typically undergo transformation and
49   consumption, which alters their sinking velocity and organic matter content and ultimately
50   reduces the carbon flux (Martin et al., 1987). The most rapid reduction in carbon flux occurs in
51   the mesopelagic zone, the region between the bottom of the productive layer and 1000 m depth
52   (Iversen et al., 2010; Stemmann et al., 2004). How much and where exactly this reduction occurs
53   determines how long the carbon is removed from the atmosphere, with transport to deeper
54   depths leading to greater storage (Kwon et al., 2009) and lower levels of atmospheric partial
55   pressure of CO_2.

56   Sinking particles provide the base of the food web for many organisms resident in the
57   mesopelagic zone, such as microbes and non-migrating zooplankton (Jackson, 1993).
58   Consumption by microbes typically leads to a reduction of the sinking particle flux through
59   dissolution and respiration of the organic carbon within the particles. Larger organisms, such as
60   zooplankton, can cause a reduction in flux via fragmentation, consumption and respiration of
61   the particles, but may also enhance sinking particle flux via the production of faster sinking
62   faecal pellets (Steinberg and Landry, 2017; Turner, 2015). In addition, abiotic processes, such as
63   disaggregation of fragile particles or aggregation of colliding particles, change particle fluxes
64   (Burd and Jackson, 2009).

65   Regardless of the exact mechanism, the mass balance of particle flux has to be conserved at
66   steady state. In other words, the attenuation (loss) of carbon flux over a defined depth interval,
67   plus the carbon transported to this depth interval via e.g. physical transport (Boyd et al., 2019),
68   should equal the accumulation of carbon within that depth interval in the form of non-sinking
69   carbon (e.g. via respiration as CO_2, solubilisation/ dissolution, incorporation into biomass or
70   transformation to other forms of non-sinking matter). Such mass balance appears, however,
71   elusive with many studies failing to reconcile carbon flux attenuation with biological activity
72   (Baltar et al., 2009; Boyd et al., 1999; Burd et al., 2010; Reinthaler et al., 2006; Steinberg et al.,
73   2008; Uchimiya et al., 2018). The first balanced carbon budget for the mesopelagic zone was
74   observed in the temperate North Atlantic (Giering et al., 2014). Intriguingly, the budget at this
75   site could only be balanced when the entire mesopelagic zone was considered: the depth-
76   resolved budget showed an excess supply of carbon (i.e. more flux attenuation than non-sinking
77   carbon accumulation) in the upper mesopelagic zone, and a deficit in the lower mesopelagic
78   (Giering et al., 2014). There was no clear reason for this imbalance, and suggested explanations
79   included vertical changes in the ecosystem with depth or an undetermined vertical transfer.

80   One of the key assumptions of the North Atlantic carbon budget was that the system was at
81   steady state (Giering et al., 2014). For large parts of the ocean, this assumption is problematic
82   due to strong seasonal cycles in export fluxes (Henson et al., 2015), which can lead to
83   misestimates of carbon supply via sinking particles of up to 25% (Giering et al., 2017). In
84   addition, in non-steady state conditions, carbon reservoirs in the interior ocean, such as non-
85   sinking organic matter accumulated at depth from previous export or subduction events (Boyd

2

86 et al., 2019; Dall'Olmo and Mork, 2014), may serve as a food source for the organisms living
87 there (e.g. Calleja et al., 2019), and hence need to be considered in carbon budgets.

88 Here, we address the scale of this accumulation and subsequent consumption of non-sinking
89 particulate matter in the mesopelagic zone in order to test the hypothesis that it serves as an
90 important food source for the mesopelagic biota and so needs to be considered for carbon
91 budgets. We further investigated whether depth-resolved budgets under non-steady state
92 conditions show the previously observed mismatch of excess supply of carbon relative to
93 consumption in the upper mesopelagic zone (and vice versa in the lower mesopelagic zone). To
94 do so, we collected high-resolution vertical profiles of carbon concentrations and fluxes in the
95 mesopelagic during a Southern Ocean spring bloom near South Georgia.

2 | Material and Methods

2.1 | Study site and sampling strategy

98   Particle profiles were collected as part of the COMICS Programme (Controls over Ocean
99   Mesopelagic Interior Carbon Storage) (Sanders et al., 2016) on the RRS Discovery. The first
100 cruise (DY086) targeted the phytoplankton spring bloom downstream of South Georgia in the
101 northern Scotia Sea in Nov/Dec 2017. The study site was chosen to be near the long-term
102 observation station 'P3' (52.4 °S, 40.1°W (Manno et al., 2015)). Because of the island-derived
103 iron supply, the region is a biological productivity and carbon flux hot spot compared to the
104 surrounding high nutrient, but low chlorophyll (HNLC) Southern Ocean (Atkinson et al., 2001;
105 Borrione and Schlitzer, 2013). The cruise was deliberately centred in an area of low current
106 speed, weak mesoscale variability and retentive circulation between the Polar Front (to the
107 West and North) and the Southern Antarctic Circumpolar Current Front (to the South) (Matano
108 et al., 2020; Meredith et al., 2003; Venables et al., 2012). We visited P3 three times for ~7 days
109 each: 15 Nov – 22 Nov (P3A), 29 Nov – 5 Dec (P3B), and 9 Dec – 15 Dec 2017 (P3C).

110
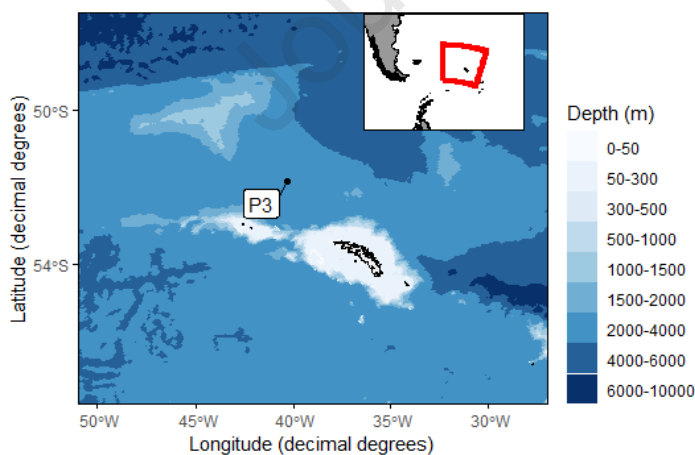
112 **Figure 1.** Long-term observation station 'P3' (52.4 °S, 40.1°W) in the vicinity of South Georgia.
113 Plotted using *ggOceanMaps* **(Mikko, 2022)**.

114

2.2 | Standard water sampling and Stand-alone pumping system (SAPS)

Concentrations of particulate organic carbon (POC) were measured from 12 CTD profiles and 5 SAPS profiles. Water samples for POC concentrations were collected from 12 depths (approximately 5, 20, 40, 50, 75, 100, 150, 250, 350, 500, 750 and 1000 m depth) using Niskin bottles fitted onto a stainless steel CTD rosette. 1000 or 2000 mL were filtered onto pre-combusted (400°C, 12 h) GF/F filters (0.7-μm nominal pore size, 25 mm, Whatman), briefly rinsed with MilliQ water to remove salts, dried (50°C, overnight) and analysed on shore. On shore, the filters were fumed with HCl (35%, 24 h), dried (50°C, >24 h), and pelleted in tin discs (Elemental microanalysis). The samples were analysed for POC using a Thermo Fisher Scientific FLASH 2000 Organic Elemental Analyser. POC calibration was performed at the beginning of each batch using a series of caffeine standards of varying weights (1 – 5 mg) with known percentage content of carbon. Reference standards were included in each batch after every 10 samples to check the instrument precision (< 1%, n = 72, 1 SD) and drift. If needed, a drift correction was applied. All samples were corrected for filter blanks. As the adsorption of dissolved organic carbon was not measured, 10.9 μg of carbon was subtracted from each POC bottle measurement (based on mean absorption found by (Cetinić et al., 2012)).

We further determined POC concentrations of two size classes (<53 μm and >53 μm) using in situ large-volume filtration. Stand Alone Pump Systems (SAPS; Challenger Oceanic) were deployed at five depths between 5 and 500 m depth and filtered, on average, 412 L (between 66 - 738 L depending on deployment depth). A full description of the methods and data interpretation is published by Preece et al. (in prep.).

2.3 | Marine Snow Catchers (MSC)

Profiles of suspended, slow-sinking and fast-sinking particles were collected using the Marine Snow Catcher (MSC) (Giering et al., 2016; Riley et al., 2012). During each visit, three particle profiles were collected with 4-5 depths chosen based on the mixed layer depth (MLD). Typically, these depths were: MLD + 10 m, MLD + 50 m, MLD + 100 m, 250 m and 500 m. Opportunistically, other depths (in the upper 250 m or at 1000 m) were also sampled. All MSCs for an individual profile were deployed within 2 h of each other, though variability between profiles collected during each visit was low. Profiles were collected during daylight hours except for two occasions (deployments to 60 m and 150 m on 18th Dec 2017). A full description of how the MSC is deployed and sampled is described by Giering et al. (2016) with slight modifications. Most notably, a tray (polypropylene, 18.5 cm diameter, 4 cm height with a total volume of ~1 L) was secured to the bottom of the base section to collect the 'fast-sinking' fraction.

Briefly, after a 2-h settling period, suspended particles were collected from the middle tap (4-5 L; 'top'). To drain the top section, the middle tap was opened fully and the bottom tap opened by approximately 30 degrees to reduce resuspension of slow-sinking material. Draining typically took 30 min. Slow-sinking particles were collected by carefully syphoning the water from above the tray (4-5 L, 'base'). The tray, containing the fast-sinking particles (1 L, 'tray', was then sealed with a lid, removed, and stored at 2–4 °C until further analysis. We did not observe any large aggregates (marine snow; > 0.5 mm diameter) until the end of the cruise; however, the fast-sinking fraction was visibly enriched in organic matter. Each fraction was filtered and analysed for POC as for standard water samples (Section 2.2). Typical filter volumes were 1000 mL for suspended and slow-sinking particles, and 150 - 350 mL for fast-sinking particles.

Concentrations of suspended, slow-sinking and fast-sinking particles (p_{sus}, p_{slow}, and p_{fast}, respectively) were calculated as follows.

4

160         $p_{sus} = p_{top}$

161         $p_{slow} = (p_{base} - p_{top}) \times V_{base} / V_{MSC}$

162         $p_{fast} = (p_{tray} - p_{base}) \times V_{tray} / (A_{tray} \times h_{MSC})$

163 Where p is the particle concentration ($\mu g\ L^{-1}$) in the top, base or tray sample, V_{base} is the volume
164 of the base section (8 L), V_{MSC} is the volume of the MSC (95 L including base), V_{tray} is the volume
165 of the tray ($\sim$ 1 L, measured for each deployment), A_{tray} is the area of the tray (0.026 m^2) and
166 h_{MSC} is the height of the MSC (1.58 m).

167 Fluxes of slow-sinking and fast-sinking particles (F_{slow} and F_{fast}, respectively) were calculated as

168         $F_{slow} = p_{slow} \times V_{MSC} / (A_{MSC} \times t)$

169         $F_{fast} = p_{fast} \times v_{fast}$

170 where A_{MSC} is the area of the MSC base (0.06 m^2), t is the settling time (2 h), and v_{fast} is the
171 average sinking velocity of the fast-sinking fraction, which we here assumed a range of sinking
172 velocities. As upper bound for the flux estimates, we applied a sinking velocity of 60 m d^{-1} based
173 on particle-specific in situ sinking velocity measurements at 500 m depth (66 ± 47 m d^{-1};
174 particle diameter of 0.5 - 2.3 mm; Iversen, pers. comm) and Polonium-derived sinking velocities,
175 which indicate bulk velocities (i.e. weighted average velocity of slow- and fast-sinking particles)
176 of 44-58 m d^{-1} at 60 m depth and increasing up to 163-182 m d^{-1} at 350 m depth (Villa-Alfageme
177 et al. this issue). An absolute lower flux estimate (i.e. F_{slow} + F_{fast}) was calculated by assuming
178 that the observed concentration gradient in the MSC developed within exactly 2 hours
179 (equivalent to a sinking velocity v_{fast} of 18 m d^{-1}), which is an underestimate because (1) a
180 substantial fraction of particles likely arrived in the base section much sooner, (2) any
181 turbulences created during sampling would have reduced the apparent concentration gradient
182 between top and base section and hence flux estimates.

183 **2.4 | PELAGRA sediment traps**
184 Flux profiles between $\sim$90 and 500 m were further measured using neutrally buoyant sediment
185 traps (PELAGRA) (Lampitt et al., 2008). PELAGRA sampling cups were filled with 10%
186 formaldehyde hypersaline solution and collected material for $\sim$24 hours. On shore, samples
187 were split into quarter subsamples (Folsom splitter; Aquatic Research Instruments) and
188 zooplankton swimmers removed. One quarter subsample was further split to obtain a final
189 subsample (either 1/16th or 1/64th) for POC analysis following the methods described above
190 (Section 2.2) with slight modifications. Subsamples were filtered onto pre-combusted (500°C
191 overnight) and pre-weighed GF/F filters (0.7-μm nominal pore size, 25 mm diameter,
192 Whatman), rinsed with buffered MilliQ water (0.025 g/L of disodium tetraborate, anhydrous
193 Fisher Scientific), and dried (40°C, overnight) for on-shore analysis. On shore, POC samples were
194 fumed (35% HCl, overnight), dried (50°C, overnight), and pelleted using tin discs (30 mm,
195 Elementar). Blanks of the trap preservative were created by filtering 30 mL of preservative onto
196 a GF/F and handling in the same way as the samples. POC was analysed at the Stable Isotope
197 Facility, University of Southampton on an Elementar Vario Isotope Select. The limit of detection
198 for the instrument was 4.88 μg of C and the analytical precision was <1%. The tin capsules had a
199 mean blank value below the detection limit of the instrument. Filter blanks (pre-combusted,
200 rinsed with borate-buffered MilliQ) had a mean blank value of 17.3 ± 2.4 μg of C. Acetanilide
201 standards were run at the beginning and end of each run and algae (bladderwrack, 1.25 ± 0.02

202 % N and 33.67 ± 0.29 % C, Elemental Microanalysis) standards followed by a blank were run
203 every five samples to track instrument performance.

204 POC fluxes (F in mg C m^{-2} d^{-1}) were calculated by normalising to the collection area of the
205 PELAGRAs (0.115 m^2) following equation, $F = m (t A)^{-1}$, where m is the carbon mass (in mg), t is
206 the collection time (in days), and A is the surface area of the opening of the collection funnel (in
207 m^2).

2.5 | Glider-derived POC concentrations and fluxes

209 Three gliders surveyed the study region between October 2017 and February 2018 as part of
210 the GOCART project (Gauging ocean Organic Carbon fluxes using Autonomous Robotic
211 Technologies). A full description of the glider mission, capabilities and data are published by
212 Henson et al. (this issue). For this study, we are focussing solely on the time period of the cruise
213 and on data from the optical backscattering sensor (at 700 nm). Henson et al. (this issue)
214 provide a comprehensive description of the method on how POC fluxes were derived from the
215 glider data. Briefly, we used a running minimum-maximum filter to isolate spikes (i.e. 'large
216 particles') from a baseline signal (i.e. 'small particles') following Briggs et al. (2011). Spikes
217 below a minimum threshold based on deep ocean 'blanks' were set to zero, eliminating some
218 instrument noise and discretization effects. This value was equivalent to particles with a
219 diameter of approximately 420 μm (following the approximate scaling between spike height
220 and size; Briggs et al. 2013), so the 'large particle' signal is interpreted as representing particles
221 >420 μm. 'Small particles' and 'large particles' were each binned into 10-m depth and 12-h time
222 bins. POC concentrations were calculated using a linear regression between backscatter and
223 CTD bottle data (15 calibration casts resulting in a final n = 141; for POC analysis methods see
224 Section 2.2; for the regression details see Henson et al., this issue). Glider-derived POC
225 concentrations and POC concentrations measured from physical samples agreed well
226 (Supplementary Fig. S1). Bulk sinking velocities of the 'large particles' were estimated using the
227 plume-tracking method (Briggs et al., 2020, 2011) with a modification to allow an increase in
228 sinking velocities with increasing depth (Villa-Alfageme et al., this issue). Resulting bulk 'large-
229 particle' sinking velocities ranged from ~40 m d^{-1} in the surface to ~130 m d^{-1} at 1000 m. The
230 sinking velocity of 'small particles' was assumed to be 2.5 m d^{-1} (sinking rate for large diatoms
231 (Bannon and Campbell, 2017)). POC flux was then calculated by multiplying POC concentrations
232 with sinking velocities and summing 'small particle' and 'large particle' fluxes. Lower and upper
233 estimates were calculated by varying the sinking velocities: For the lower estimate, sinking
234 velocities for 'small particles' and 'large particles' were set to 0 m d^{-1} and 50% of the 'best
235 estimate', respectively. For the upper estimate, 'small particles' and 'large particles' were set to
236 10 m d^{-1} (Briggs et al., 2020)and 100% of the 'best estimate', respectively. The estimates of the
237 deepest glider bin (990 – 1000 m; nominally 995 m) has the highest uncertainties because the
238 glider turned at this depth and the motion of the particles through the backscattering sensor
239 was hence less reliable. We therefore used the next deepest bin (980 – 1000 m; nominal 985 m)
240 as representative deep flux.

241
2.6 | Calculation of vertical and temporal changes

243 We used the glider-derived high-resolution POC concentration and flux data to investigate
244 spatiotemporal changes. Specifically, we aimed to calculate the change in POC concentration at
245 any specific depth range and to estimate the POC fraction that can be accounted for by the input
246 of material to the depth range of interest. To quantify the change in POC concentration within

247 each depth bin over time ('temporal changes'), we calculated the difference from one 12-h bin to
248 the next, and then calculated the average change in POC concentration for each visit. This value
249 is the average rate of change in POC concentration during each visit (~7 days) and is expressed
250 in absolute terms (mg C m^{-3} d^{-1}) or as percentage daily change (d^{-1}) of the average POC
251 concentration (in mg C m^{-3}) during that period. We calculated the absolute difference in POC
252 concentration within each depth bin relative to the average concentration of that depth bin (in
253 mg C m^{-3}) throughout the study period (15 Nov 2017 - 15 Dec 2017). Finally, we calculated the
254 vertical difference in POC concentrations (in mg C m^{-3}) for each POC profile by subtracting the
255 concentration at a given depth bin from the highest POC concentration of that profile.

256 For fluxes, we quantified the 'vertical changes' for each profile by subtracting the deeper depth
257 bin, which was expected to have a lower flux following flux attenuation, from the depth bin
258 immediately above (e.g. flux [bin 30-40 m] - flux [bin 40-50 m]) and dividing by the bin size
259 (i.e., 10 m; resulting in unit mg C m^{-3} d^{-1}). We then calculated the average of each depth bin for
260 each visit and computed the running mean (n = 5) to reduce the noise. The resulting values
261 showed the average vertical change during each visit (~7 days) and can be expressed in
262 absolute terms (mg C m^{-3} d^{-1}) or percentage daily change (d^{-1}) of the average POC concentration
263 (in mg C m^{-3}) during that period.

2.7 | Export depth based on productive layer
265 The depth of export, and hence the boundary between epipelagic and mesopelagic zone, was
266 here chosen to be the productive layer depth. The productive layer is the layer in which
267 particles can be produced photosynthetically and is typically either the euphotic zone depth or
268 the mixed layer depth, whichever is deeper (Dall'Olmo and Mork, 2014). Following the
269 recommendations by Buesseler et al. (Buesseler et al., 2020), we estimated the productive layer
270 depth from the glider time-series (Henson et al., this issue) using a modification of the metric by
271 Owens et al. (Owens et al., 2015). For each glider profile, the productive layer depth was defined
272 as the deepest point at which chlorophyll was higher than 10% of the maximum chlorophyll
273 concentration for that profile. During the cruise period, the estimated productive layer depths
274 were always deeper than the euphotic zone (0.1% PAR) and exceeded the seasonal mixed layer
275 depth (0.05 kg m^{-3} density difference from surface values) by a median value of 13 m.

276 The estimated export depths were 92.5 m ± 8.1 m, 91.5 m ± 12.9 m and 88.5 m ± 10.4 m for the
277 first, second and third visit, respectively. As the glider-derived high-resolution POC
278 concentrations and fluxes were binned in 10-m bins, we used the bin 90-100 (nominal '95 m')
279 as export depth throughout the manuscript.

3 | Results
3.1 | POC concentrations
282 The glider backscatter-derived POC concentrations generally matched observations between
283 the mixed layer and 500 m depth (Fig. 2 & 3). The glider may have underestimated POC
284 concentrations in the mixed layer and below 500 m compared to CTD bottle data. In the mid-
285 water column, the CTD-derived POC concentrations appeared slightly higher and SAPS-derived
286 a bit lower. Overall the high-resolution backscatter-derived POC profiles appear to describe the
287 observed vertical profiles well. Hereafter, POC concentrations will refer to the high-resolution
288 glider backscatter-derived values unless otherwise stated.

289 POC concentrations showed the typical vertical gradient with higher concentrations in the
290 surface ocean (142-252 mg C m^{-3} at 0-10 m) and a rapid decline in the upper mesopelagic to 24-

291   40 mg C m^{-3} at 190-200 m depth. Below this depth, POC concentrations declined slowly to 7-9
292   mg C m^{-3} at ~1000 m depth (Fig. 3). Over the course of the cruise, POC concentrations in the
293   surface (0-10 m) declined from 252 to 181 to 142 mg C m^{-3} during the first, second and third
294   visit to P3, respectively. This decline concurred with a decrease in the phytoplankton
295   community in terms of chlorophyll concentrations in the mixed layer (from 3.8 ± 1.9 mg Chl m^{-3}
296   during the first visit to 1.3 ± 0.3 mg Chl m^{-3} during the third visit) (Ainsworth et al., 2023).
297   Throughout the cruise, the phytoplankton community was dominated by large cells (>10 μm),
298   composed predominantly of diatoms such as *Eucampia Antarctica* and *Fragilariopsis*
299   *kerguelensis*, which made up ~95%, ~91% and ~83% of the total chlorophyll in the mixed layer
300   during the first, second and third visit, respectively (Ainsworth et al., 2023).

301   Conversely, POC concentrations in the upper mesopelagic increased during this time, from 24 to
302   39 to 40 mg C m^{-3} (at 190-200 m depth). These opposing trends along each depth horizon are
303   clearly illustrated by the temporal anomalies with a change exceeding -120 mg C m^{-3} in the
304   surface ocean (Fig. 4a). As a result of the opposing trends, the initially strong vertical
305   concentration gradient, with a decrease of up to 268 mg C m^{-3} from the surface to 1000 m depth
306   during P3A, became much weaker (Fig. 4b). Towards the end of the third visit (P3C), the
307   concentration gradient from surface to 1000 m depth had decreased to 130 mg C m^{-3}. An
308   average of only 4% of the estimated glider-derived POC concentration (over the entire cruise
309   period and between 95 and 1000 m depth) was associated with 'large particles' (>420 μm in
310   diameter), which agreed well with the scarcity of visible aggregates (>500 μm diameter) in the
311   Marine Snow Catchers.

312   The high-resolution data further allowed us to calculate rates of change during each visit (i.e.
313   the average rate of change during ~7 days). In the mixed layer, changes were erratic with no
314   clear trend. Throughout the mesopelagic zone, POC concentrations increased during the first
315   and second visit (P3A and P3B; Fig. 5a). During P3B, the average daily increase during the visit
316   was up to 1.2 mg C m^{-3} d^{-1} at 150-170 m depth, equivalent to a daily increase of 2.6% d^{-1} of the
317   POC standing stock (Fig. 5b). This accumulation reversed during our third visit (P3C), when POC
318   concentrations decreased at an average rate of up to -0.8 mg C m^{-3} d^{-1} at 250-270 m depth,
319   equivalent to -2.7% d^{-1} of the POC standing stock at this depth (Fig. 5b).
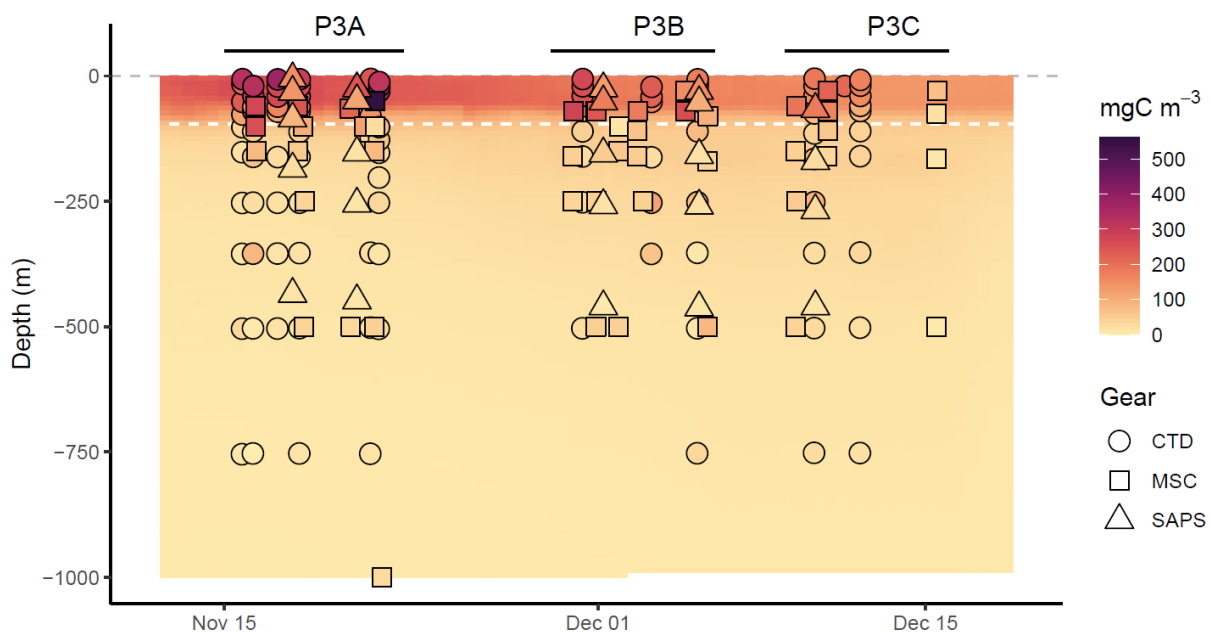
320

321 **Figure 2.** POC concentrations in the mesopelagic during the cruise (range: 0-550 mg C m^{-3}) based on
322 samples collected using Niskin bottles ('CTD' as circles), Marine Snow Catchers ('MSC' as squares) and
323 stand-alone pumping systems ('SAPS' as triangles). Background shows POC concentrations based on
324 glider backscatter intensity. Sampling periods during visits P3A, P3B and P3C are indicated by the
325 horizontal bars. White dashed line indicates the mixed layer depth.

326

327
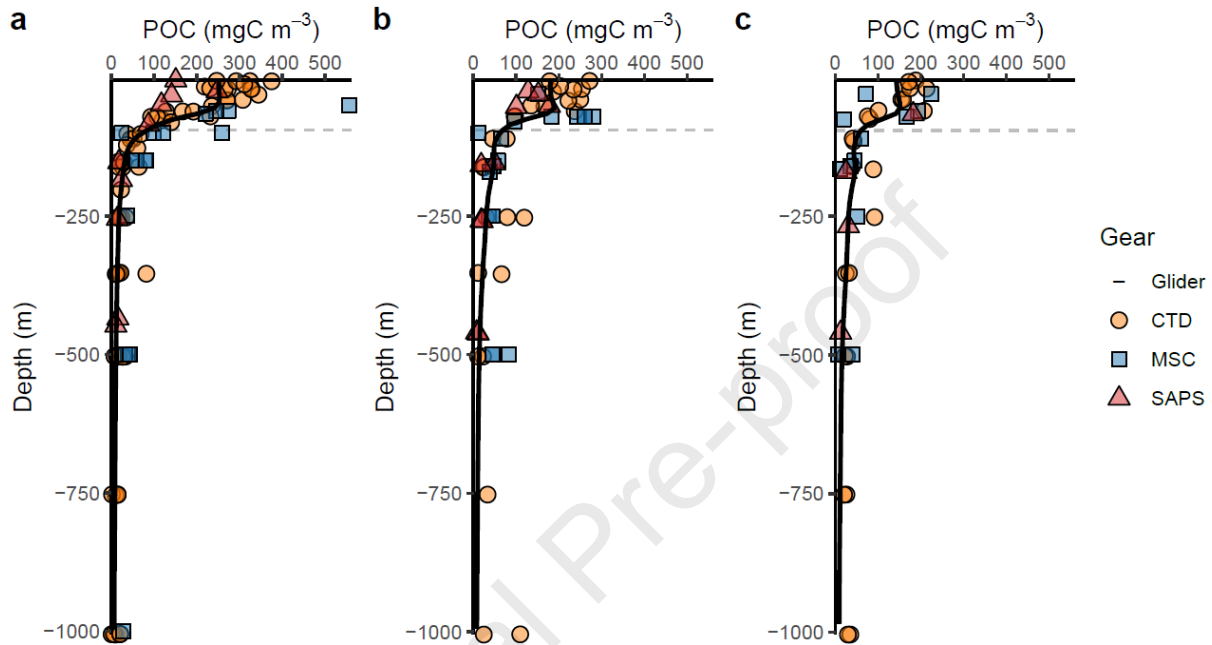
328

329 **Figure 3.** Vertical profiles of POC concentrations during the three station occupations. (a) P3A: Nov – 22
330 Nov, (b) P3b: 29 Nov – 5 Dec, and (c) P3C 9 Dec – 15 Dec 2017. Symbols identify data source: CTD bottle
331 data (open circle), glider-derived (solid line), MSC time-zero samples (open square), and SAPS filter (open
332 triangle). Grey dashed line indicates the mixed layer depth.

9

333

334
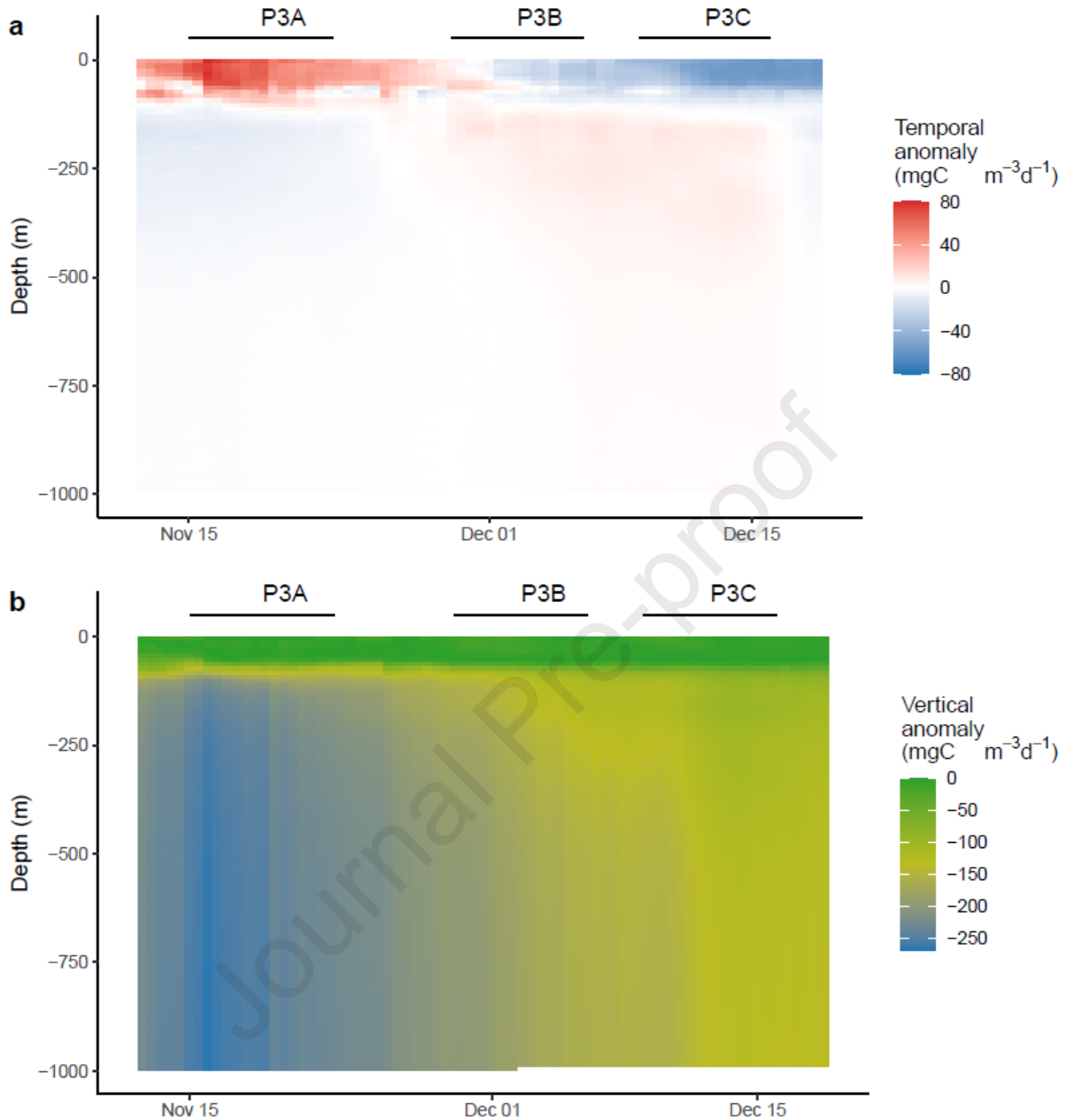
Figure 4. Change in POC concentrations. (a) Change over time at a given depth normalized to the average
concentration at that depth (in 10-m bins). Red indicates a period of higher POC concentration relative to
the average at this depth; blue indicates a period of lower POC concentration. (b) Change of POC
concentration with depth relative to the surface concentration. Green shades indicate similar
concentrations as those at the surface, yellow shades indicate a difference of ~ 150 mg C m^{-3}, blue shades
indicate a difference of ~ 250 mg C m^{-3} relative to the surface.

341

342
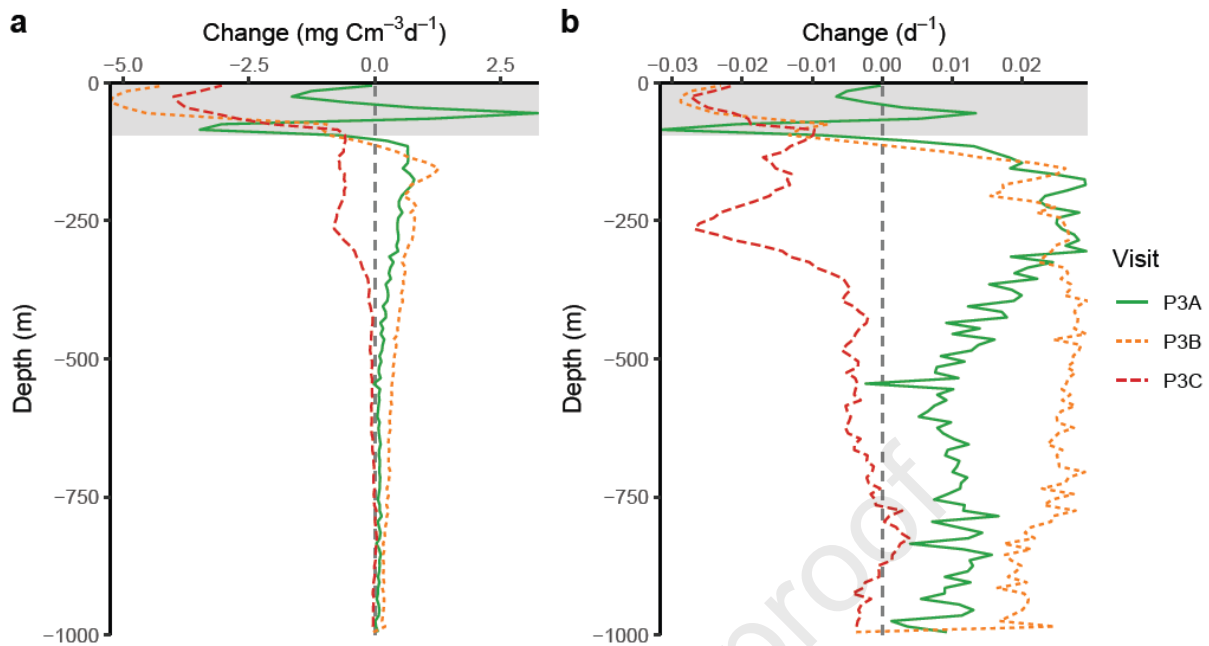
Figure 5. Change in POC concentration at depth over the duration of the visit expressed as (a) absolute mass (mg C m^{-3} d^{-1}), and (b) fraction of the average POC concentration during that period at that depth (d^{-1}). I.e. the value at 250 m refers to the change of POC concentration at this depth over a 24-h period. Visits P3A, P3B and P3C are shown in solid green, dotted orange and dashed red, respectively. The mixed layer is shaded in grey.

3.2 | POC fluxes

The time-series revealed an overall good match of the glider-derived POC flux estimates and the direct measurements (Fig. 6; Henson et al. this issue). All platforms seemed to agree well around 500 m depth, though near the surface there were some distinct differences. The PELAGRA traps estimated fluxes toward the lower end of the glider-derived uncertainty envelope, with largest discrepancies near the mixed layer depth during P3A and P3C. This observation is in line with previous observations that sediment traps tend to underestimate flux in the upper ocean owing to a range of factors, such as hydrodynamic disturbances and dissolution (Buesseler et al., 2007). Furthermore, the conical shape of the PELAGRA trap might have led to undersampling of small particles throughout the water column (Baker et al., 2020). A comparison of the two size classes of POC determined by the SAPS revealed a significant increase in larger particles (> 53 μm) with depth from 20% of total POC in the upper 100 m (range: 7-37%) to 41% of total POC between 400 - 500 m depth (range: 31-53%; p = 0.03, R2 = 0.15, n = 24). MSC-derived flux estimates, on the other hand, were towards the upper end of the glider-derived uncertainty envelope. Noteworthy here is the uncertainty range for the MSC: the open squares indicate the minimum "true fluxes" based on the concentration gradient observed after 2 hours of settling (Fig. 7), whereas the blue squares consider fast-sinking particles that had likely arrived in the bottom section in shorter than two hours. The MSC uncertainty envelope generally straddled the glider-derived best estimate, suggesting overall good agreement between the two estimates. Hence, hereafter, POC fluxes will refer to the high-resolution backscatter-derived values unless otherwise stated.

371   POC fluxes followed the typical pattern of high fluxes in the surface ocean (755 - 1435 mg C m^{-2}
372   d^{-1} at 50-60 m depth) that were attenuated rapidly in the upper mesopelagic (from 287 - 646
373   mg C m^{-2} d^{-1} at 90-100 m to 141-215 mg C m^{-2} d^{-1} at 190-200 m depth) and more slowly in the
374   lower mesopelagic (down to 56-74 mg C m^{-2} d^{-1} at 980-990 m depth) (Fig. 7). Throughout the
375   cruise, POC export (defined as flux at 95 m) declined from 646 to 409 to 287 mg C m^{-2} d^{-1} during
376   the first, second and third visit, respectively (Table 1). This change in flux broadly mirrored the
377   decline in primary production (1948 ± 89, 1488 ± 146 and 1221 ± 56 mg C m^{-2} d^{-1} during the
378   first, second and third visit, respectively; Henson et al., this issue) estimated from incubation
379   experiments and glider-derived light fields based on methods by Mignot et al. (2018). Export
380   efficiencies (export flux as a fraction of net primary production) appeared to decrease over time
381   (33, 27 and 24%, respectively).

382   Flux attenuation in the upper mesopelagic was highest during the first visit with changes of up
383   to 19 mg C m^{-3} d^{-1} (equivalent to 0.22 d^{-1} of the POC concentration) just below the export depth
384   (Fig. 8). The magnitude of this attenuation decreased during the cruise, down to 11 mg C m^{-3} d^{-1}
385   (equivalent to 0.15 d^{-1} of the POC concentration) just below the export depth during the third
386   visit (Fig. 8). The vertical pattern of flux attenuation was not consistent, with higher attenuation
387   rates being maintained much deeper (to ~165 m depth, as defined at the first occurrence when
388   flux attenuation was <2 mg C m^{-3} d^{-1}) during the first visit compared to the second and third
389   visit (to 125 m and 115 m depth, respectively) (Fig. 8a). As a result, transfer efficiency
390   throughout the upper 100 m of the mesopelagic (from 95 to 195 m depth) increased during the
391   cruise from 22 to 53 to 64% during the first, second and third visit, respectively. Transfer
392   efficiency through the remainder of the mesopelagic zone (i.e. from 195 to 985 m depth)
393   decreased throughout the cruise, from 52% during the first visit to 34 and 30% during the
394   second and third visit, respectively (Table 1).

395

396

397
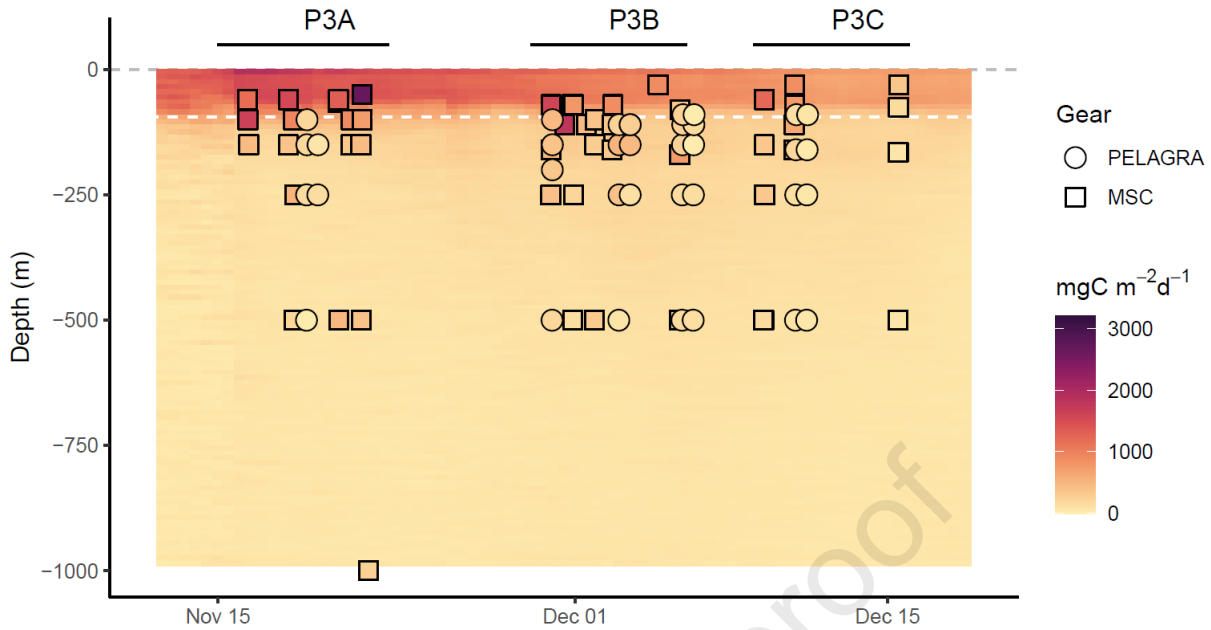
Figure 6. Time series of vertical flux profiles during the cruise (13th Nov - 18th Dec 2017). Background shading shows fluxes derived based on the glider backscatter. Overlaid are fluxes determined by the Marine Snow Catchers (MSC, squares) and PELAGRA sediment traps (circles). White dashed line indicates the mixed layer depth.

402


403
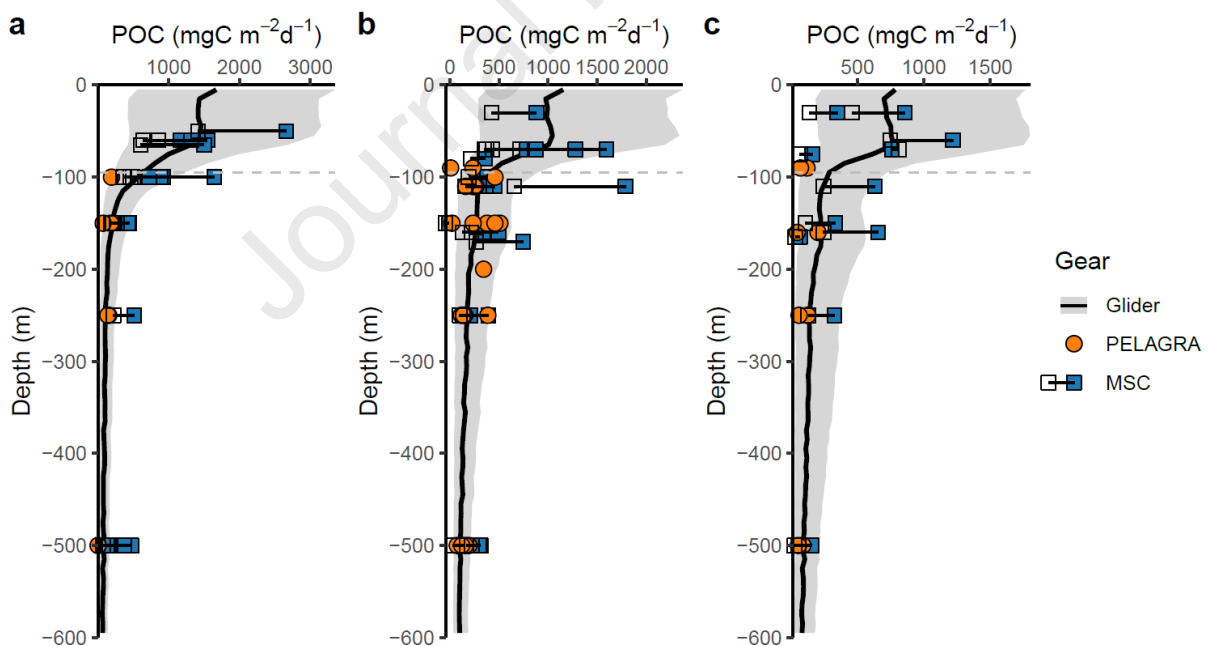
Figure 7. Vertical flux profiles during the three visits at (a) P3A, (b) P3B and (c) P3C. Black line shows glider-based estimates with lower and upper limits indicated by the grey envelope. Overlaid are fluxes determined by the Marine Snow Catchers (MSC, squares) and PELAGRA sediment traps (orange circles). The absolute lower flux estimate based on the MSCs is indicated by the open squares, whereas the blue squares show their best estimate.

409
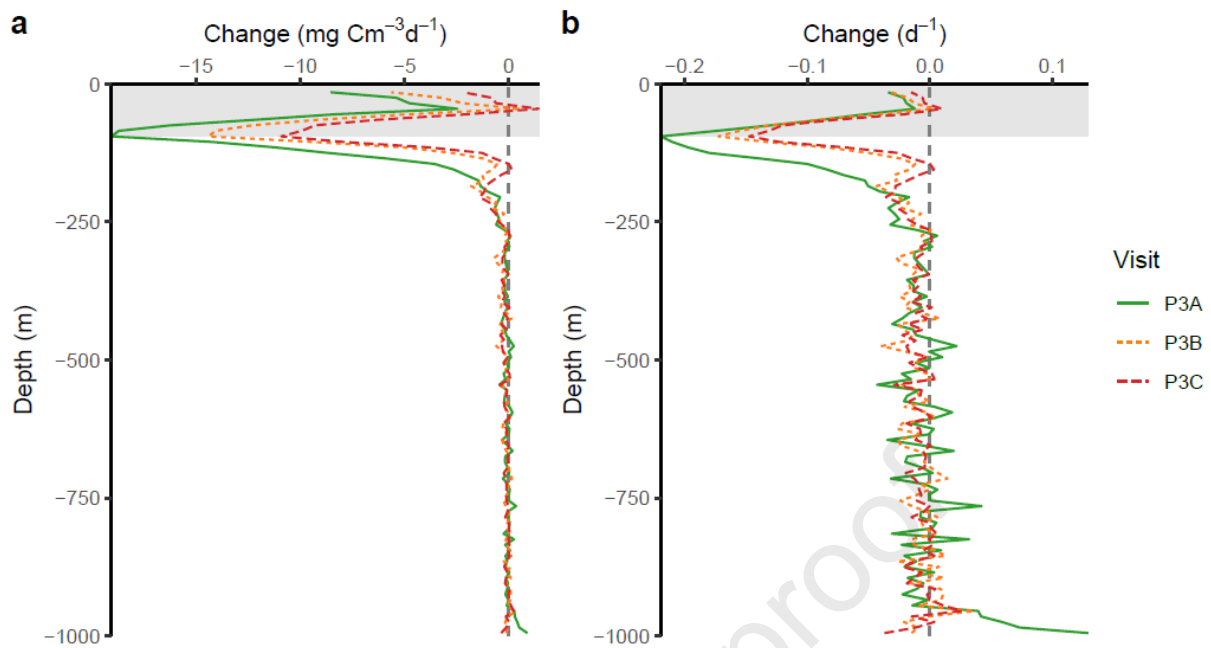
Figure 8. Change in vertical POC flux with depth during each visit expressed as (a) absolute mass (mg C m^{-3} d^{-1}), and (b) fraction of POC concentration at that depth (d^{-1}). I.e., the value at 250 m refers to the change of POC flux from 249 m depth to the flux at 250 m depth. Visits P3A, P3B and P3C are shown in solid green, dotted orange and dashed red, respectively. The mixed layer is shaded in grey.

Table 1. Overview of the visits. Primary production (PP) based on incubation experiments and glider-derived chlorophyll and lightfields. Fluxes are based on glider-derived estimates. Export efficiency (ExEff) is the ratio of export flux over PP. The shallow transfer efficiency, T_{100}, is the fraction of export flux that makes it to 100 m below export depth (i.e. 195 m). The lower mesopelagic transfer efficiency, $T_{lowerMZ}$, is the fraction of sinking material that reaches 1000 m depth relative to flux at 195 m.

| Visit	PP (0- 60 m)	'Export': Flux at 95 m	Flux at 195 m	Flux at 985 m	ExEff	T_{100}	$T_{lowerMZ}$
	mg C m^{-2} d^{-1}	mg C m^{-2} d^{-1}	mg C m^{-2} d^{-1}	mg C m^{-2} d^{-1}			
P3A	1948	646	141	74	0.33	0.22	0.52
P3B	1488	409	215	73	0.27	0.53	0.34
P3C	1221	287	185	56	0.24	0.64	0.30

3.3 | POC budgets

We compared the attenuation in flux (i.e. how much of the flux was 'lost' to, e.g., respiration, fragmentation, etc.) with the change in stock (i.e. whether the POC concentrations increased or decreased). Integrated over the entire mesopelagic and in the upper mesopelagic (95-195 m), POC flux attenuation was higher than the observed accumulation of suspended POC during all three visits (Fig. 9a). Between 95 and 1000 m, during the first, second and third visit, respectively, flux attenuation (581, 388 and 302 mg C m^{-2} d^{-1}) exceeded the accumulation of POC

429   in this depth interval (197, 366 and -172 mg C m^{-2} d^{-1}; equivalent to 34, 94 and -57% of the flux

430   attenuation), leaving an excess of 384, 22 and 474 mg C m^{-2} d^{-1} for respiration (and dissolution).

431   Excess was even more pronounced in the upper mesopelagic (95 - 195 m), where flux

432   attenuation (520, 253 and 170 mg C m^{-2} d^{-1}) exceeded POC accumulation (63, 67 and -63 mg C

433   m^{-2} d^{-1}; equivalent to 12, 27 and -37% of the flux attenuation) and allowed 457, 186 and 233 mg

434   C m^{-2} d^{-1} for other consumptive processes. However, in the lower mesopelagic, POC flux

435   attenuation during the first and second visit did not supply sufficient carbon to even explain the

436   increase in suspended POC (Fig. 9c): Flux attenuation supplied 61 (uncertainty envelope: 10-

437   186) and 135 (30-361) mg C m^{-2} d^{-1} during the first and second visit, respectively, whereas POC

438   accumulation appeared to be 134 (122-147) and 299 (270-327) mg C m^{-2} d^{-1}. Hence, there

439   seemed to be a deficit of 74 and 164 mg C m^{-2} d^{-1}, though it is noteworthy that the estimates

440   match within the uncertainties. During the third visit, POC stocks appeared to decrease (-109

441   mg C m^{-2} d^{-1}), hence allowing a total of 241 mg C m^{-2} d^{-1} for consumptive processes over this

442   depth horizon. The budgets are robust in respect of the exact separation depth between upper

443   and lower mesopelagic (Supplementary Fig. S2)

444

445
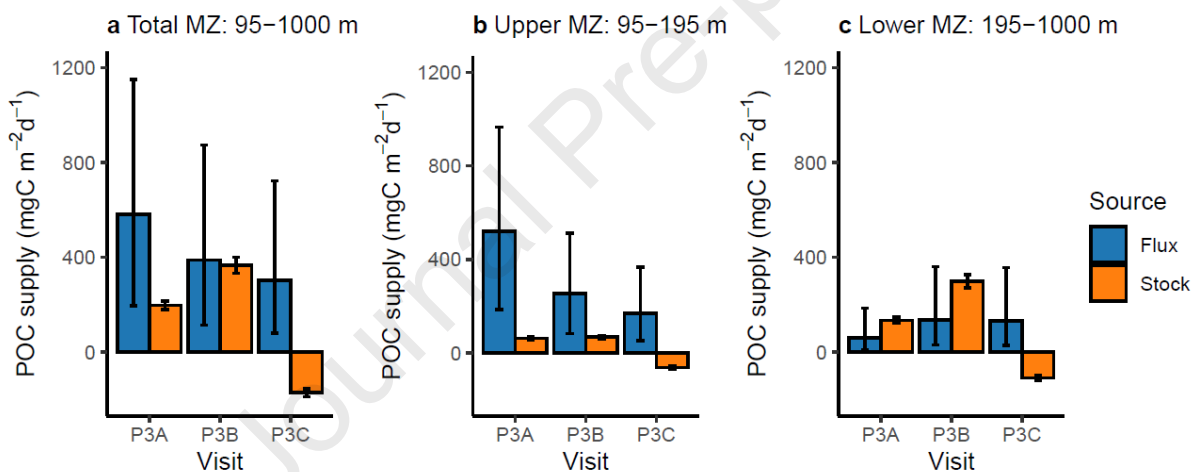
447   **Figure 9.** Mesopelagic carbon budget with different depth horizons. Comparison of organic matter

448   supply via sinking particles (blue) to the accumulation (or loss at P3C) of POC (orange) during the three

449   visits (P3A, P3B and P3C) for **(a)** the entire mesopelagic zone from 95-1000 m depth, **(b)** the upper

450   mesopelagic zone from 95 - 195 m depth, and **(c)** the lower mesopelagic zone from 195 - 1000 m depth.

451   Values (mg C m^{-2} d^{-1}) are integrated over the three depth horizons (905, 100 and 805 m, respectively).

452   Error bars show, for fluxes, upper and lower estimates for fluxes based on sinking rate assumptions, and,

453   for stocks, standard deviation of estimated POC concentrations.

454

4 | Discussion

456   We compared high-resolution estimates of gravitational POC flux and accumulation of POC

457   within the mesopelagic over the course of the spring bloom. First, we explore the temporal

458   changes in the POC inventory of the mesopelagic zone under non-steady state conditions and

459   discuss the implications for ocean carbon storage via the biological pump. We then focus on the

460   vertical distribution of these changes by compiling simple carbon budgets. We did not include

461   respiration in our budgets as the estimation of mesopelagic respiration introduces large

462   uncertainties (e.g. Giering et al., 2014; Giering and Evans, 2022). While, at face value, the
463   budgets balance when considering the entire mesopelagic with excess carbon for respiration, a
464   vertical transfer of carbon from the upper to the lower mesopelagic appears to be needed,
465   particularly when we factor in that respiration by prokaryotes and zooplankton occurred
466   (Evans et al., this issue; Cook et al., this issue). We discuss the potential transport mechanisms
467   that could help resolve this vertical imbalance.

468   **4.1 | Effect of spring bloom on mesopelagic environment**
469   The mesopelagic is typically considered an oligotrophic environment owing to its relatively low
470   resource availability, with POC concentrations typically similar to those observed in surface
471   water of oligotrophic regions (25 mg C m^{-3}; Supplementary Fig. 3) (Martiny et al., 2014), which
472   we also observed during our first visit. Here, however, we observed a strong enrichment in POC
473   concentrations throughout the cruise (up to 46 mg C m^{-3} at 165 m during the third visit),
474   equivalent to levels observed in temperate surface waters (Martiny et al., 2014). This
475   accumulation was likely driven by the high amount of organic matter that was exported from
476   the mixed layer throughout the bloom. Export fluxes during our first visit (646 mg C m^{-2} d^{-1})
477   were on the high end of observed global export fluxes (Henson et al., 2015; Mouw et al., 2016).
478   Though high, these fluxes were consistent with the high primary production rates measured
479   during our study ($\sim$ 2000 mg C m^{-2} d^{-1} during the first visit; Henson et al., this issue). The
480   resulting export efficiency, i.e. the ratio of export over primary production, of 24-33% was
481   consistent with large-scale satellite-derived estimates for our study region (20-30% (Henson et
482   al., 2012); though see (Arteaga et al., 2018) for a comparison of satellite-derived estimates).

483   In terms of temporal changes, the mesopelagic is often considered at steady state with any
484   particulate organic matter entering it meeting one of two fates: (1) it stops sinking through
485   fragmentation or consumption and is converted to dissolved carbon (as either dissolved organic
486   carbon or dissolved inorganic carbon) or (2) it leaves the mesopelagic as part of the sinking
487   particle flux. Here, in addition to these processes, we observed that a substantial fraction of the
488   particulate flux (34-94%) appeared to have slowed down or stopped sinking and accumulated
489   as particulate matter in the upper mesopelagic zone. This accumulation is consistent with
490   observations in the Nordic Sea ($\sim$70°N 3°E) of a seasonal accumulation of small particles in the
491   mesopelagic (Dall'Olmo and Mork, 2014). Moreover, it is consistent with estimates of particle
492   fragmentation rates during high-flux events in the North Atlantic and Indian sectors of the
493   Southern Ocean (30-60%) (Briggs et al., 2020).

494   The gliders observed a concomitant increase in fluorescence down to 400 m depth (Henson et
495   al., this issue), suggesting that the accumulated POC was associated, at least in part, with
496   relatively fresh phytoplankton. Measurements of fast repetition rate fluorescence (Kolber et al.,
497   1998) on the material collected by the sediment traps at 500 m during the second visit (2nd
498   Dec) suggested that it contained phytoplankton cells with photosynthetic efficiencies (0.33 ±
499   0.02 F_v/F_m) similar to those found near the surface (0.3-0.4 F_v/F_m; Moore et al., unpublished).
500   On-board incubations of surface phytoplankton communities in complete darkness showed that
501   even after 16 days (end of incubation) the phytoplankton cells continued to be
502   photosynthetically viable without a marked decrease in their physiological status (from $\sim$ 0.36
503   F_v/F_m to $\sim$ 0.31 F_v/F_m) (Moore et al., unpublished). In addition, ship-board radiotracer
504   experiments indicated that mesopelagic microbes were likely not remineralizing sinking
505   healthy diatom cells (Ainsworth et al., 2023). Hence, active phytoplankton cells could have spent

506 a considerable time sinking through the mesopelagic before undergoing remineralization owing
507 to consumption or cell depth.

508 Only a relatively small fraction (22%) of the exported material was transferred through the
509 upper mesopelagic (95-195 m depth) during the first visit, indicating that particle sinking
510 velocities slowed down. During this period, we did not observe any large aggregates (>0.5 mm
511 diameter) in the MSCs but instead a high abundance of large diatoms and diatom chains (visual
512 inspection and in situ camera systems; Giering et al., 2020). Though we cannot conclusively say
513 why these particles slowed down and eventually stopped sinking, it was probably a
514 combination of vertical changes in seawater density (e.g. MacIntyre et al., 1995), particle
515 buoyancy regulation of viable cells like diatoms (e.g. Moore and Villareal, 1996), dissolution and
516 microbial remineralization (e.g. Benner and Amon, 2015; Hansell and Orellana, 2021), and
517 fragmentation or disaggregation (Briggs et al., 2020). The slow-down in sinking velocities of
518 these particles in the upper mesopelagic would lead to a gross accumulation in POC, as observed
519 here. It would further explain why particles became more homogeneous in appearance (such as
520 size, roundness and solidity) towards the lower mesopelagic (Giering et al., 2020): the
521 proportion of denser, non-viable particles would become relatively more important for flux
522 with depth.

523 The accumulation of organic matter in the upper mesopelagic was, however, transient, as it only
524 occurred during the first two visits, after which we observed a decrease of the accumulated POC
525 (Fig. 5). Overall, mesopelagic POC concentrations appeared to follow the pattern of surface
526 ocean seasonality, albeit delayed by approximately 2-3 weeks. Glider-derived primary
527 production showed peak production rates during and just after the first visit (P3A; around 17th
528 - 29th Nov) (Henson et al., this issue), whereas POC concentrations in the upper mesopelagic
529 peaked around 3rd - 13th Dec (Fig. 4a). One may hence consider two different phases: a net
530 accumulative phase when particle flux attenuation delivered more carbon than was lost due to
531 heterotrophic and dissolution processes, followed by a net consumptive phase when both
532 particle flux and carbon stock were drawn down, i.e., consumed. During the consumptive phase,
533 the 'reservoir' of suspended POC supplied carbon equivalent to 32-82% of the flux supply (Fig.
534 9). This reservoir is typically not considered for mesopelagic carbon budgets, which are often
535 considered to be at steady-state (e.g. Collins et al., 2015; Giering et al., 2014; Santana-Falcón et
536 al., 2017; Steinberg et al., 2008).

537 We propose that, as the system was in non-steady state, the whole mesopelagic ecosystem was
538 likely not very active during the first visit (P3A) as indicated by low microbial activity (lowest
539 observed leucine assimilation rates throughout the cruise; Rayne et al., this issue). As a result,
540 any sinking matter in the mesopelagic zone could escape consumption. This effect would not be
541 apparent in the upper mesopelagic where particles may have slowed down or stopped sinking
542 from processes other than consumption. It is, however, in line with the observation that transfer
543 efficiency in the lower mesopelagic was highest during P3A: 52% of the sinking material was
544 transferred from 195 to 1000 m depth (Table 1).

545 As the bloom progressed, three things appeared to have happened. (1) The surface ocean
546 changed to a more heterotrophic system as indicated by the decline in primary production and
547 POC concentrations in the surface ocean (Fig. 2,4) and the increase in prokaryotic activity
548 (Rayne et al., this issue). This increase in heterotrophic activity may have resulted in more
549 tightly packed, faster sinking particles. Based on in situ imaging data (holographic camera; see
550 Giering et al. (2020)), the proportion of detritus- and faecal-pellet-like particles was highest

551 during the third visit: The contribution of clearly identifiable diatoms decreased from 30% to
552 13% estimated carbon biomass (average between 1-255 m depth), while detritus-like particle
553 biomass increased from 65 to 77% (Giering, unpublished data). Note, however, that
554 zooplankton biomass did not appear to have changed over the course of the study (Cook et al.,
555 this issue). (2) These more compact, likely faster sinking particles appeared to have sunk
556 through the upper 100 m of the mesopelagic zone relatively unperturbed (in terms of quantity)
557 during the second and third visits, with a transfer efficiency T_{100} of 53-64%. (3) By the time of
558 the second visit, the mesopelagic ecosystem appeared to have 'switched on': during P3B and
559 P3C, the transfer through the lower part of the mesopelagic zone ($T_{lowerMZ}$) decreased to ~30-
560 34%. (Note, the rates are on top of the consumption of suspended POC). This increased activity
561 was likely caused by microbial activity: microbial biomass, leucine uptake, leucine respiration
562 and leucine assimilation efficiencies - which can be used as proxy for growth efficiencies - had
563 increased throughout the mesopelagic zone (Rayne et al., this issue).

564 The resulting effect is peculiar: regardless of the time of the bloom, rates of PP and size of export
565 flux, the flux that reached 1000 m depth was relatively constant throughout the cruise (56-74
566 mg C m^{-2} d^{-1}). If this phenomenon was widespread, our observation would have direct
567 implications for estimating the strength of the biological carbon pump in the Southern Ocean. In
568 particular, the use of surface conditions (e.g., satellite-derived parameters such as primary
569 production or export efficiency) to estimate ocean carbon storage would likely overestimate the
570 impact of surface blooms for transporting carbon to depth.

571 **4.2 | Mesopelagic POC budgets - unresolved vertical transfer**
572 Our POC budgets showed a similar vertical separation in the dynamics of the upper and the
573 lower mesopelagic as observed in the North Atlantic (Giering et al., 2014). For the North
574 Atlantic budget, the mesopelagic was, as in our case, separated at 100 m below the mixed layer
575 (i.e. upper and lower mesopelagic = 50-150 m and 150-1000 m, respectively), making both
576 studies directly comparable. In both cases, the use of a dynamic upper boundary for the
577 mesopelagic (see also Buesseler and Boyd, 2009) was critical for correctly assessing the
578 mesopelagic carbon budget (Giering et al., 2014). A similar vertical mismatch between source
579 and sink was also observed in the subarctic and subtropical western North Pacific for 200-500
580 m vs 500-4810 m during several short (< 1 month) field campaigns (Uchimiya et al., 2018). The
581 latter study suggested that the vertical uncoupling can be partially resolved by "*assuming a
582 temporal uncoupling between supply and consumption, which partly equilibrates the carbon
583 budget over a longer (yearly) time scale*" (Uchimiya et al., 2018). A steady-state assumption over
584 a longer time scale (yearly) may also be valid in our study region. However, in our case, we
585 directly accounted for temporal mismatch in POC supply and consumption by tracking
586 mesopelagic POC accumulation, and we still found that measured POC supply by sinking flux is
587 likely insufficient to explain the lower mesopelagic budget in two of the three visits (Fig. 9c).
588 While this mismatch does not quite exceed the uncertainty bounds of our POC flux supply
589 estimates, even our upper bound supply estimates, which only just match the observed
590 accumulation during visits P3A and P3B, would not leave any room in the lower mesopelagic
591 budget for POC consumption. Hence we find a mismatch in our mesopelagic POC budgets that is
592 logistical rather than temporal.

593 In addition to temporal decoupling, another suggested cause for the apparent vertical mismatch
594 in previous studies was related to methodological issues concerning the estimates of
595 respiration: Typically, carbon budgets assume that metabolic conversion factors are constant

596   throughout the deep ocean (e.g. Giering et al. 2014). Subtle changes in ecosystem structure, such
597   as decreasing microbial communities and activity, with depth (DeLong et al., 2006; Iversen et al.,
598   2010) could however cause depth variations in the conversion factors and hence introduce
599   apparent over- and underestimates of the true activities. Here, our budgets are based solely on
600   POC flux vs. stock and estimates of respiration are not included. In our case, methodological
601   uncertainties include our flux estimation and any associated parameters that may change with
602   depth. Our POC dataset is in itself consistent as it uses the same method (glider-derived POC)
603   and conversion factors. Backscatter-to-POC conversion factors may differ for suspended and
604   sinking particles and with depth. If aggregates of surface POC material dominate the large-
605   particle signal, this difference is expected to be small (Briggs et al., 2011) and unlikely to
606   introduce mismatches of the order observed here (see also Supplementary Fig. S1). In theory,
607   compact faecal pellets could scatter less light per unit mass than suspended particles
608   (decreasing b_{bp}/POC), but they might also be depleted in organic carbon relative to "fresh"
609   material (increasing b_{bp}/POC). While the conversion of backscatter-to-POC may change with
610   depth and hence may increase uncertainties, bottle POC measurements also suffer from higher
611   inaccuracies at depth owing to the relatively larger effect of contamination of blank signals
612   when concentrations are low. Despite these caveats, our glider-derived estimates of POC
613   concentrations agreed well with direct observations (Fig. 2&3). For the exploration of POC
614   concentrations at depth, we believe that the combination of high-resolution optically derived
615   data with more traditional methods such as bottle samples are best.

616   Methodological uncertainties are higher around the sinking velocity estimates. We applied
617   sinking velocities for large particles that increased with depth and were consistent with
618   independent estimates of sinking velocities (Villa-Alfageme et al., this issue), and we carried out
619   a sensitivity analysis. The resulting fluxes agreed reasonably well with independent flux
620   observations (Fig. 6&7). Consequently, methodological issues with sinking POC flux estimates
621   are unlikely to be the primary cause for the observed vertical imbalance. Another source of
622   uncertainty in our budgets is the potential effect of advection on our mesopelagic net
623   accumulation budgets. The study was conducted in an area of low current speed (Matano et al.,
624   2020), and minimal changes in mesopelagic temperature and salinity were observed over the
625   course of the study (*data not shown*). Therefore we do not expect advection to explain the
626   substantial discrepancy between lower mesopelagic POC supply and accumulation in two of the
627   three cruise periods.

628   Hence, the most likely explanation is an unaccounted mechanism that vertically transfers
629   carbon from the upper to the lower mesopelagic (as also suggested by Giering et al., 2014). Five
630   mechanisms that can inject particles into the ocean interior have been identified (Boyd et al.,
631   2019) that we have not considered so far, namely the mixed-layer pump, the large-scale
632   physical pump, the eddy-subduction pump, the seasonal-lipid pump and the mesopelagic-
633   migrant pump.

634   The large-scale physical pump describes the transport of particles by large-scale (>100 km)
635   subduction through Ekman pumping and circulation features and is typically small relative to
636   carbon transport by sinking particles (Boyd et al., 2019). Moreover, though our study site was
637   close to the Southern Antarctic Circumpolar Current Front (Matano et al., 2020), our study site
638   was, according to global models, located in a region of low subduction rates (Liu and Huang,
639   2012). Particles can also be subducted by eddies, a mechanism called the eddy-subduction
640   pump (Boyd et al., 2019). The study site, located in a region with a retentive circulation and

641   weak mesoscale activity (Matano et al., 2020), experienced low current speeds (< 0.06 m s^{-1};
642   Henson et al., this issue). During our study, we did not observe evidence of subsurface advection
643   (based on high-resolution salinity and temperature profiles obtained with the gliders; Henson et
644   al., this issue), indicating that eddy subduction was negligible. The exception was a temporary
645   advection signal from the 16th Dec 2017 onwards, which was apparent in both the glider profiles
646   (see also Fig. 4a) as well as in satellite data (*not shown*). However, this date was after the end of
647   our last visit to the study site (P3C), indicating that our budgets were likely observing a quasi-
648   1D system.

649   The mixed-layer pump (Gardner et al., 1995) typically occurs during the early phases of the
650   spring bloom, during the winter-spring transition, before the onset of seasonal stratification:
651   Periods of weak stratification that promote surface primary production are interspersed with
652   periods of weather-driven short-term mixing, which transports the new biomass to depth
653   (Dall'Olmo and Mork, 2014; Giering et al., 2016). In our study region, recurrent wind-driven
654   thermal restratification events shaped the phytoplankton bloom in the region (Carvalho, in
655   prep/pers. comm.). Yet, we observed a strengthening of the mixed layer rather than a
656   weakening as would be required for the mixed layer pump. Furthermore, though we observed
657   periodic restratification events throughout cruise, potentially leaving phytoplankton biomass at
658   depth while a new mixing layer started, we did not see active mixing below the seasonal MLD
659   ~70 m (Carvalho, in prep./pers. comm.). The remnant winter water (100-200 m depth, Carmack
660   & Foster (1975)), characterised by temperature minimum, likely acted as a physical barrier for
661   deep vertical mixing. We hence consider it unlikely that the mixed-layer pump contributed
662   notably to the redistribution of the carbon within the mesopelagic zone.

663   The seasonal-lipid pump concerns the annual phenomenon of copepods, a type of zooplankton,
664   migrating to depth for hibernation over the winter (Jónasdóttir et al., 2015). As our study was
665   carried out during the spring, this pump was likely not applicable here.

666   Finally, larger zooplankton and fish are known to migrate between the surface ocean and the
667   mesopelagic zone, and these organisms can hence redistribute organic matter in the form of
668   biomass, excretion and egestion products (mesopelagic-migrant pump) (Steinberg and Landry,
669   2017). Often, migration occurs synchronised following the day-night pattern, and carbon export
670   via this diel vertical migration (DVM) can be equivalent to 40% of total carbon export (Brierley,
671   2014). However, during our study, we did not observe signs of synchronous DVM in total
672   biomass or acoustic backscatter (Cook et al., this issue), and only a few individual groups
673   appeared at consistently higher biomass at depth during the day (the copepod *Metridia* spp.,
674   salps, fish and decapods; Cook et al., this issue). Other migration patterns include reverse
675   synchronous DVM, when populations migrate to the surface ocean during the day (e.g. Ohman et
676   al. 1983), sporadic synchronous vertical migration, when populations do not migrate every day
677   (e.g. Darnis et al., 2017), and asynchronous migration, when individuals of the same group
678   migrate independently (e.g. Cottier et al., 2006). A lack of classical DVM has been observed
679   during the main season of primary production in high-latitude regions (e.g. Darnis et al., 2017),
680   and migration behaviour may be adapted depending on the environmental conditions (Bandara
681   et al., 2021; Cresswell et al., 2009). Hence, the vertical transfer during our study may have
682   occurred via a mix of migration patterns that concealed the extent of overall migration.

683   We can explore whether migration could have transported sufficient carbon to depth by
684   carrying out a rough calculation. Mesozooplankton (>330 μm) and micronekton (>4 mm)
685   biomass was ~15,000 mg C m^{-2} (0-62 m depth) and 300 mg C m^{-2} (0-250 m depth), respectively

686 (Cook et al., this issue). The deficit between POC flux supply and stock accumulation in the lower
687 mesopelagic during P3A and P3B (74 and 164 mg C m^{-2} d^{-1}, respectively; Figure 9) was hence
688 equivalent to ~ 0.5-1.1% of the mesozooplankton biomass and 25-55% of the micronekton
689 biomass. Though the amount that mesozooplankton ingest daily ranges from <1 to 150% of
690 their body weight (e.g. (Castellani et al., 2008; Cowles and Fessenden, 1995; Mayor et al., 2006)
691 Cook et al., this issue), only a small fraction of the ingested material would be carried to depth
692 before egestion there. For micronekton, this 'gut flux' has been estimated to be 40% of the
693 respired carbon (see refs in Hernández-León et al., 2019), and we assume the same percentage
694 for mesozooplankton here. Respiration and excretion by common vertical migrators
695 (subtropical North Atlantic) are, respectively, 10% (range 3-22%) and 4% (range 1-10%)
696 (Steinberg et al., 2000). Gut flux by mesozooplankton and micronekton could hence have been
697 ~600 mg C m^{-2} d^{-1} (range 180-1320 mg C m^{-2} d^{-1}) and ~12 mg C m^{-2} d^{-1} (range 3.6 - 26.4 mg C m^{-2}
698 d^{-1}), provided the entire community migrated. In addition, migrators would have released
699 additional carbon through excretion, which could have fuelled prokaryotic biomass production
700 via the microbial loop. Assuming migrators spent 12 hours at depth, an additional 300 mg C m^{-2}
701 d^{-1} (range 75-750 mg C m^{-2} d^{-1}) and 6 mg C m^{-2} d^{-1} (range 1.5-15 mg C m^{-2} d^{-1}) may have been
702 excreted by mesozooplankton and micronekton, respectively. When combining the mid-
703 estimates of both gut flux and excretion, 8-18% of the surface mesozooplankton community or
704 4-9 times the surface micronekton community would have had to migrate to transport sufficient
705 carbon to the lower mesopelagic zone to balance our lower mesopelagic carbon budgets.
706 Asynchronous vertical migration hence remains as a possible transfer mechanism.

707 In conclusion, we cannot conclusively explain the vertical transfer observed here with any of the
708 mechanisms known to us. Note though, that the budget deficit in the lower mesopelagic was
709 relatively small compared to the excess in the upper mesopelagic. Overall, the vertical
710 imbalance in mesopelagic carbon budgets remains an exciting knowledge gap that is waiting to
711 be explained.

5a| Acknowledgements

5b| Funding sources

5c| Author contribution

728 **Giering:** Conceptualization, Methodology, Formal analysis, Investigation, Validation,
729 Visualization, Writing

730   **Sanders:** Conceptualization, Funding acquisition, Investigation, Writing,
731   **Blackbird:** Sample analysis
732   **Briggs:** Methodology, Investigation, Validation, Writing
733   **Carvalho:** Methodology, Investigation, Validation, Writing
734   **East:** Sample analysis, Data curation, Investigation
735   **Espinola:** Sample analysis, Investigation
736   **Henson:** Conceptualization, Writing
737   **Kiriakoulakis:** Sample collection
738   **Iversen:** Sample collection, Writing
739   **Lampitt:** Conceptualization, Sample collection
740   **Pabortsava:** Sample analysis
741   **Pebody:** Sample analysis
742   **Peele:** Sample analysis
743   **Preece:** Sample analysis
744   **Saw:** Engineering, Methodology
745   **Villa-Alfageme**: Investigation, Writing
746   **Wolff:** Investigation, Writing

6 | References

From Special Issue:

Henson, S., Briggs, N., Carvalho, F., Manno, C., Mignot, A., Thomalla, S., 2022. Seasonal variability in biological carbon pump efficiency in the northern Scotia Sea, Southern Ocean. This issue.

Preece, C., Blackbird, S., Kiriakoulakis, K., Tarling, G. A., Cook, K., Mayor, D. J., Atherden, F., Giering, S. L. C., Stowasser, G., Wolff, G., A., 2022. Insights into the fate of particulate organic matter in the mesopelagic zone, Scotia Sea, Southern Atlantic Ocean. In preparation.

Rayne, R. R.-P., Giering, S. L. C., Hartmann, M., Sanders, R., Evans, C., 2022. Insights into prokaryotic carbon and energy limitation in the epi and mesopelagic from leucine supply and assimilation efficiency during a POC export event. This issue.

Villa-Alfageme, M., Briggs, N., Ceballos-Romero, E., de Soto, F., Manno, C., Giering, S. L. C., 2022. Seasonal variations of sinking velocities in Austral diatom blooms: Lessons learned from COMICS I. This issue.

Published:

Ainsworth, J., Poulton, A.J., Lohan, M.C., Stinchcombe, M.C., Lough, A.J.M., Moore, C.M., 2023. Iron cycling during the decline of a South Georgia diatom bloom. Deep Sea Research Part II: Topical Studies in Oceanography 208, 105269. https://doi.org/10.1016/j.dsr2.2023.105269

Arteaga, L., Haëntjens, N., Boss, E., Johnson, K.S., Sarmiento, J.L., 2018. Assessment of Export Efficiency Equations in the Southern Ocean Applied to Satellite-Based Net Primary Production. Journal of Geophysical Research: Oceans 123, 2945–2964. https://doi.org/10.1002/2018JC013787

Atkinson, A., Whitehouse, M.J., Priddle, J., Cripps, G.C., Ward, P., Brandon, M.A., 2001. South Georgia, Antarctica: A productive, cold water, pelagic ecosystem. Marine Ecology Progress Series 216, 279–308. https://doi.org/10.3354/meps216279

Baker, C.A., Estapa, M.L., Iversen, M., Lampitt, R., Buesseler, K., 2020. Are all sediment traps created equal? An intercomparison study of carbon export methodologies at the PAP-SO site. Progress in Oceanography 184, 102317. https://doi.org/10.1016/j.pocean.2020.102317

Baltar, F., Aristegui, J., Gasol, J.M., Sintes, E., Herndl, G.J., 2009. Evidence of prokaryotic metabolism on suspended particulate organic matter in the dark waters of the subtropical North Atlantic. Limnology and Oceanography 54, 182–193.

Bandara, K., Varpe, Ø., Wijewardene, L., Tverberg, V., Eiane, K., 2021. Two hundred years of zooplankton vertical migration research. Biological Reviews 96, 1547–1589. https://doi.org/10.1111/brv.12715

Bannon, C.C., Campbell, D.A., 2017. Sinking towards destiny: High throughput measurement of phytoplankton sinking rates through time-resolved fluorescence plate spectroscopy. PLOS ONE 12, e0185166. https://doi.org/10.1371/journal.pone.0185166

Benner, R., Amon, R.M.W., 2015. The Size-Reactivity Continuum of Major Bioelements in the Ocean. Annual Review of Marine Science 7, 185–205. https://doi.org/10.1146/annurev-marine-010213-135126

Borrione, I., Schlitzer, R., 2013. Distribution and recurrence of phytoplankton blooms around South Georgia, Southern Ocean. Biogeosciences 10, 217–231. https://doi.org/10.5194/bg-10-217-2013

Boyd, P.W., Claustre, H., Levy, M., Siegel, D.A., Weber, T., 2019. Multi-faceted particle pumps drive carbon sequestration in the ocean. Nature 568, 327–335. https://doi.org/10.1038/s41586-019-1098-2

Boyd, P.W., Sherry, N.D., Berges, J.A., Bishop, J.K.B., Calvert, S.E., Charette, M. a., Giovannoni, S.J., Goldblatt, R., Harrison, P.J., Moran, S.B., Roy, S., Soon, M., Strom, S., Thibault, D., Vergin, K.L., Whitney, F. a., Wong, C.S., 1999. Transformations of biogenic particulates from the pelagic to the deep ocean realm. Deep Sea Research II 46, 2761–2792. https://doi.org/10.1016/S0967-0645(99)00083-1

Brierley, A.S., 2014. Diel vertical migration. Current Biology 24, R1074–R1076. https://doi.org/10.1016/j.cub.2014.08.054

Briggs, N., Dall'Olmo, G., Claustre, H., 2020. Major role of particle fragmentation in regulating biological sequestration of CO 2 by the oceans. Science 367, 791–793. https://doi.org/10.1126/science.aay1790

Briggs, N., Perry, M.J., Cetinić, I., Lee, C., D'Asaro, E., Gray, A.M., Rehm, E., 2011. High-resolution observations of aggregate flux during a sub-polar North Atlantic spring bloom. Deep Sea Research Part I: Oceanographic Research Papers 58, 1031–1039. https://doi.org/10.1016/j.dsr.2011.07.007

Buesseler, K.O., Boyd, P.W., 2009. Shedding light on processes that control particle export and flux attenuation in the twilight zone of the open ocean. Limnology and Oceanography 54, 1210–1232. https://doi.org/10.4319/lo.2009.54.4.1210

Buesseler, K.O., Antia, A.N., Chen, M., Fowler, S.W., Gardner, W.D., Gustafsson, O., Harada, K., Michaels, A.F., van der Loeff, M., Sarin, M., others, Loeff, M.R.V.D., Sarin, M., 2007. An assessment of the use of sediment traps for estimating upper ocean particle fluxes. Journal of Marine Research 65, 345–416.

Buesseler, K.O., Boyd, P.W., Black, E.E., Siegel, D.A., 2020. Metrics that matter for assessing the ocean biological carbon pump. Proceedings of the National Academy of Sciences 117, 9679–9687. https://doi.org/10.1073/pnas.1918114117

Burd, A.B., Hansell, D. a., Steinberg, D.K., Anderson, T.R., Arístegui, J., Baltar, F., Beaupré, S.R., Buesseler, K.O., DeHairs, F., Jackson, G. a., Kadko, D.C., Koppelmann, R., Lampitt, R.S., Nagata, T., Reinthaler, T., Robinson, C., Robison, B.H., Tamburini, C., Tanaka, T., 2010. Assessing the apparent imbalance between geochemical and biochemical indicators of meso- and bathypelagic biological activity: What the @$♯! is wrong with present calculations of carbon budgets? Deep Sea Research II 57, 1557–1571. https://doi.org/10.1016/j.dsr2.2010.02.022

Burd, A.B., Jackson, G.A., 2009. Particle Aggregation. Annual Review of Marine Science 1, 65–90. https://doi.org/10.1146/annurev.marine.010908.163904

Calleja, M.Ll., Al-Otaibi, N., Morán, X.A.G., 2019. Dissolved organic carbon contribution to oxygen respiration in the central Red Sea. Sci Rep 9, 4690. https://doi.org/10.1038/s41598-019-40753-w

Carmack, E.C., Foster, T.D., 1975. On the flow of water out of the Weddell Sea. Deep Sea Research and Oceanographic Abstracts 22, 711–724. https://doi.org/10.1016/0011-7471(75)90077-7

Castellani, C., Irigoien, X., Mayor, D.J., Harris, R.P., Wilson, D., 2008. Feeding of Calanus finmarchicus and Oithona similis on the microplankton assemblage in the Irminger Sea, North Atlantic. Journal of Plankton Research 30, 1095–1116. https://doi.org/10.1093/plankt/fbn074

Cetinić, I., Perry, M.J., Briggs, N.T., Kallin, E., D'Asaro, E.A., Lee, C.M., 2012. Particulate organic carbon and inherent optical properties during 2008 North Atlantic Bloom Experiment. Journal of Geophysical Research: Oceans 117, n/a-n/a. https://doi.org/10.1029/2011JC007771

Collins, J.R., Edwards, B.R., Thamatrakoln, K., Ossolinski, J.E., DiTullio, G.R., Bidle, K.D., Doney, S.C., Van Mooy, B.A.S., 2015. The multiple fates of sinking particles in the North Atlantic Ocean. Global Biogeochemical Cycles 29, 1471–1494. https://doi.org/10.1002/2014GB005037

Cottier, F.R., Tarling, G.A., Wold, A., Falk-Petersen, S., 2006. Unsynchronised and synchronised vertical migration of zooplankton in a high Arctic fjord. Limnology and Oceanography 51, 2586–2599. https://doi.org/10.4319/lo.2006.51.6.2586

Cowles, T.J., Fessenden, L.M., 1995. Copepod grazing and fine-scale distribution patterns during the Marine Light-Mixed Layers experiment. Journal of Geophysical Research 100, 6677–6686.

Cresswell, K.A., Tarling, G.A., Thorpe, S.E., Burrows, M.T., Wiedenmann, J., Mangel, M., 2009. Diel vertical migration of Antarctic krill (Euphausia superba) is flexible during advection across the Scotia Sea. Journal of Plankton Research 31, 1265–1281. https://doi.org/10.1093/plankt/fbp062

Dall'Olmo, G., Mork, K.A., 2014. Carbon export by small particles in the Norwegian Sea. Geophysical Research Letters 41, 2921–2927. https://doi.org/10.1002/2014GL059244

Darnis, G., Hobbs, L., Geoffroy, M., Grenvald, J.C., Renaud, P.E., Berge, J., Cottier, F., Kristiansen, S., Daase, M., E. Søreide, J., Wold, A., Morata, N., Gabrielsen, T., 2017. From polar night to midnight sun: Diel vertical migration, metabolism and biogeochemical role of zooplankton in a high Arctic fjord (Kongsfjorden, Svalbard). Limnology and Oceanography 62, 1586–1605. https://doi.org/10.1002/lno.10519

DeLong, E., Preston, C., Mincer, T., Rich, V., 2006. Community genomics among stratified microbial assemblages in the ocean's interior. Science 311, 496–503.

Gardner, W.D., Chung, S.P., Richardson, M.J., Walsh, I.D., 1995. The oceanic mixed-layer pump. Deep Sea Research Part II: Topical Studies in Oceanography 42, 757–775. https://doi.org/10.1016/0967-0645(95)00037-Q

Giering, S.L.C., Evans, C., 2022. Overestimation of prokaryotic production by leucine incorporation—and how to avoid it. Limnology and Oceanography 67, 726–738. https://doi.org/10.1002/lno.12032

Giering, S.L.C., Hosking, B., Briggs, N., Iversen, M.H., 2020. The Interpretation of Particle Size, Shape, and Carbon Flux of Marine Particle Images Is Strongly Affected by the Choice of Particle Detection Algorithm. Frontiers in Marine Science 7, 564. https://doi.org/10.3389/fmars.2020.00564

Giering, S.L.C., Humphreys, M.P., 2018. Biological Pump, in: White W. (Eds) Encyclopedia of Geochemistry. Springer Berlin Heidelberg. https://doi.org/10.1007/978-3-319-39193-9_154-1

Giering, S.L.C., Sanders, R., Lampitt, R.S., Anderson, T.R., Tamburini, C., Boutrif, M., Zubkov, M.V., Marsay, C.M., Henson, S.A., Saw, K., Cook, K., Mayor, D.J., 2014. Reconciliation of the carbon budget in the ocean's twilight zone. Nature 507, 480–483. https://doi.org/10.1038/nature13123

Giering, S.L.C., Sanders, R., Martin, A.P., Henson, S.A., Riley, J.S., Marsay, C.M., Johns, D.G., 2017. Particle flux in the oceans: Challenging the steady state assumption. Global Biogeochemical Cycles 31, 159–171. https://doi.org/10.1002/2016GB005424

Giering, S.L.C., Sanders, R., Martin, A.P., Lindemann, C., Möller, K.O., Daniels, C.J., Mayor, D.J., St. John, M.A., 2016. High export via small particles before the onset of the North Atlantic spring bloom. Journal of Geophysical Research: Oceans 121, 6929–6945. https://doi.org/10.1002/2016JC012048

Hansell, D.A., Orellana, M.V., 2021. Dissolved Organic Matter in the Global Ocean: A Primer. Gels 7, 128. https://doi.org/10.3390/gels7030128

Henson, S.A., Sanders, R., Madsen, E., 2012. Global patterns in efficiency of particulate organic carbon export and transfer to the deep ocean. Global Biogeochemical Cycles 26, GB1028–GB1028. https://doi.org/10.1029/2011GB004099

Henson, S.A., Yool, A., Sanders, R., 2015. Variability in efficiency of particulate organic carbon export: A model study. Global Biogeochemical Cycles 29, 33–45. https://doi.org/10.1002/2014GB004965

Hernández-León, S., Olivar, M.P., Fernández de Puelles, M.L., Bode, A., Castellón, A., López-Pérez, C., Tuset, V.M., González-Gordillo, J.I., 2019. Zooplankton and Micronekton Active Flux Across the Tropical and Subtropical Atlantic Ocean. Frontiers in Marine Science 6.

Iversen, M.H., Nowald, N., Ploug, H., Jackson, G. a., Fischer, G., 2010. High resolution profiles of vertical particulate organic matter export off Cape Blanc, Mauritania: Degradation processes and ballasting effects. Deep Sea Research Part I: Oceanographic Research Papers 57, 771–784. https://doi.org/10.1016/j.dsr.2010.03.007

Jackson, G.A., 1993. Flux feeding as a mechanism for zooplankton grazing and its implications for vertical particulate flux 1. Limnology and Oceanography 38, 1328–1331.

Jónasdóttir, S.H., Visser, A.W., Richardson, K., Heath, M.R., 2015. Seasonal copepod lipid pump promotes carbon sequestration in the deep North Atlantic. Proceedings of the National Academy of Sciences 112, 12122–12126. https://doi.org/10.1073/pnas.1512110112

Kolber, Z.S., Prášil, O., Falkowski, P.G., 1998. Measurements of variable chlorophyll fluorescence using fast repetition rate techniques: defining methodology and experimental protocols. Biochimica et Biophysica Acta (BBA) - Bioenergetics 1367, 88–106. https://doi.org/10.1016/S0005-2728(98)00135-2

Kwon, E.Y., Primeau, F., Sarmiento, J.L., 2009. The impact of remineralization depth on the air-sea carbon balance. Nature Geoscience 2, 630–635. https://doi.org/10.1038/ngeo612

Lampitt, R.S., Boorman, B., Brown, L., Lucas, M., Salter, I., Sanders, R., Saw, K., Seeyave, S., Thomalla, S.J., Turnewitsch, R., 2008. Particle export from the euphotic zone: Estimates using a novel drifting sediment trap, 234Th and new production. Deep Sea Research Part I: Oceanographic Research Papers 55, 1484–1502. https://doi.org/10.1016/j.dsr.2008.07.002

Liu, L.L., Huang, R.X., 2012. The Global Subduction/Obduction Rates: Their Interannual and Decadal Variability. Journal of Climate 25, 1096–1115. https://doi.org/10.1175/2011JCLI4228.1

MacIntyre, S., Alldredge, A.L., Gotschalk, C.C., 1995. Accumulation of marines now at density discontinuities in the water column. Limnology and Oceanography 40, 449–468. https://doi.org/10.4319/lo.1995.40.3.0449

Manno, C., Stowasser, G., Enderlein, P., Fielding, S., Tarling, G.A., 2015. The contribution of zooplankton faecal pellets to deep-carbon transport in the Scotia Sea (Southern Ocean). Biogeosciences 12, 1955–1965. https://doi.org/10.5194/bg-12-1955-2015

Martin, J.H., Knauer, G.A., Karl, D.M., Broenkow, W.W., 1987. VERTEX: carbon cycling in the northeast Pacific. Deep Sea Research Part A. Oceanographic Research Papers 34, 267–285. https://doi.org/10.1016/0198-0149(87)90086-0

Martiny, A.C., Vrugt, J.A., Lomas, M.W., 2014. Concentrations and ratios of particulate organic carbon, nitrogen, and phosphorus in the global ocean. Sci Data 1, 140048. https://doi.org/10.1038/sdata.2014.48

Matano, R.P., Combes, V., Young, E.F., Meredith, M.P., 2020. Modeling the Impact of Ocean Circulation on Chlorophyll Blooms Around South Georgia, Southern Ocean. Journal of Geophysical Research: Oceans 125, e2020JC016391. https://doi.org/10.1029/2020JC016391

Mayor, D.J., Anderson, T.R., Irigoien, X., Harris, R., 2006. Feeding and reproduction of Calanus finmarchicus during non-bloom conditions in the Irminger Sea. Journal of Plankton Research 28, 1167–1179. https://doi.org/10.1093/plankt/fbl047

Meredith, M.P., Watkins, J.L., Murphy, E.J., Ward, P., Bone, D.G., Thorpe, S.E., Grant, S.A., Ladkin, R.S., 2003. Southern ACC Front to the northeast of South Georgia: Pathways, characteristics, and fluxes. Journal of Geophysical Research: Oceans 108. https://doi.org/10.1029/2001JC001227

Mignot, A., Ferrari, R., Claustre, H., 2018. Floats with bio-optical sensors reveal what processes trigger the North Atlantic bloom. Nat Commun 9, 190. https://doi.org/10.1038/s41467-

017-02143-6

Mikko, V., 2022. ggOceanMaps: Plot Data on Oceanographic Maps using "ggplot2."

Moore, J., Villareal, T., 1996. Buoyancy and growth characteristics of three positively buoyant marine diatoms. Marine Ecology Progress Series 132, 203–213. https://doi.org/10.3354/meps132203

Mouw, C.B., Barnett, A., McKinley, G.A., Gloege, L., Pilcher, D., 2016. Phytoplankton size impact on export flux in the global ocean. Global Biogeochemical Cycles 30, 1542–1562. https://doi.org/10.1002/2015GB005355

Ohman, M.D., Frost, B.W., Cohen, E.B., 1983. Reverse Diel Vertical Migration: An Escape from Invertebrate Predators. Science 220, 1404–1407. https://doi.org/10.1126/science.220.4604.1404

Owens, S.A., Pike, S., Buesseler, K.O., 2015. Thorium-234 as a tracer of particle dynamics and upper ocean export in the Atlantic Ocean. Deep Sea Research Part II: Topical Studies in Oceanography 116, 42–59. https://doi.org/10.1016/j.dsr2.2014.11.010

Parekh, P., Dutkiewicz, S., Follows, M.J., Ito, T., 2006. Atmospheric carbon dioxide in a less dusty world. Geophysical Research Letters 33, 2–5. https://doi.org/10.1029/2005GL025098

Reinthaler, T., van Aken, H.M., Veth, C., Williams, P. leB, Aristegui, J., Robinson, C., Lebaron, P., Herndl, G.J., 2006. Prokaryotic respiration and production in the meso- and bathypelagic realm of the eastern and western North Atlantic basin. Limnology and Oceanography 51, 1262–1273.

Riley, J.S., Sanders, R., Marsay, C., Le Moigne, F.A.C., Achterberg, E.P., Poulton, A.J., 2012. The relative contribution of fast and slow sinking particles to ocean carbon export. Global Biogeochemical Cycles 26, GB1026–GB1026. https://doi.org/10.1029/2011GB004085

Sanders, R.J., Henson, S.A., Martin, A.P., Anderson, T.R., Bernardello, R., Enderlein, P., Fielding, S., Giering, S.L.C., Hartmann, M., Iversen, M., Khatiwala, S., Lam, P., Lampitt, R., Mayor, D.J., Moore, M.C., Murphy, E., Painter, S.C., Poulton, A.J., Saw, K., Stowasser, G., Tarling, G.A., Torres-Valdes, S., Trimmer, M., Wolff, G.A., Yool, A., Zubkov, M., 2016. Controls over Ocean Mesopelagic Interior Carbon Storage (COMICS): Fieldwork, Synthesis, and Modeling Efforts. Frontiers in Marine Science 3, 1–7. https://doi.org/10.3389/fmars.2016.00136

Santana-Falcón, Y., Álvarez-Salgado, X.A., Pérez-Hernández, M.D., Hernández-Guerra, A., Mason, E., Arístegui, J., 2017. Organic carbon budget for the eastern boundary of the North Atlantic subtropical gyre: major role of DOC in mesopelagic respiration. Sci Rep 7, 10129. https://doi.org/10.1038/s41598-017-10974-y

Steinberg, D.K., Carlson, C.A., Bates, N.R., Goldthwait, S. a., Madin, L.P., Michaels, A.F., 2000. Zooplankton vertical migration and the active transport of dissolved organic and inorganic carbon in the Sargasso Sea. Deep Sea Research Part I: Oceanographic Research Papers 47, 137–158. https://doi.org/10.1016/S0967-0637(99)00052-7

Steinberg, D.K., Landry, M.R., 2017. Zooplankton and the Ocean Carbon Cycle. Annual Review of Marine Science 9, 413–444. https://doi.org/10.1146/annurev-marine-010814-015924

Steinberg, D.K., Mooy, B.A.S.V., Buesseler, K.O., Boyd, P.W., Kobari, T., Karl, D.M., 2008. Bacterial vs zooplankton control of sinking particle flux in the ocean's twilight zone. Limnology and Oceanography 53, 1327–1338.

Stemmann, L., Jackson, G.A., Gorsky, G., 2004. A vertical model of particle size distributions and fluxes in the midwater column that includes biological and physical processes—Part II: application to a three year survey in the NW Mediterranean Sea. Deep Sea Research Part I: Oceanographic Research Papers 51, 885–908. https://doi.org/10.1016/j.dsr.2004.03.002

Turner, J.T., 2015. Zooplankton fecal pellets, marine snow, phytodetritus and the ocean's biological pump. Progress in Oceanography 130, 205–248. https://doi.org/10.1016/j.pocean.2014.08.005

Uchimiya, M., Fukuda, H., Wakita, M., Kitamura, M., Kawakami, H., Honda, M.C., Ogawa, H., Nagata, T., 2018. Balancing organic carbon supply and consumption in the ocean's interior: Evidence from repeated biogeochemical observations conducted in the subarctic and subtropical western North Pacific. Limnology and Oceanography 63, 2015–2027. https://doi.org/10.1002/lno.10821

Venables, H., Meredith, M.P., Atkinson, A., Ward, P., 2012. Fronts and habitat zones in the Scotia Sea. Deep-Sea Research Part II: Topical Studies in Oceanography 59–60, 14–24. https://doi.org/10.1016/j.dsr2.2011.08.012

Volk, T., Hoffert, M.I., 1985. The Carbon Cycle and Atmospheric CO2: Natural Variations Archean to Present, Geophysical Monograph Series, Geophysical Monograph Series. American Geophysical Union, Washington, D. C. https://doi.org/10.1029/GM032

Supplementary material.
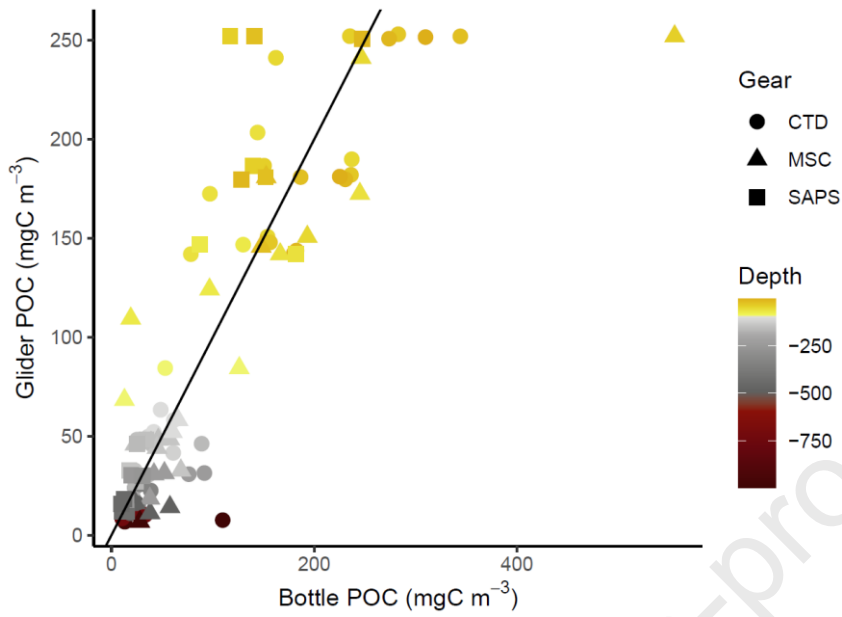
Figure S1. Correlation between glider-derived POC concentrations and POC concentrations measured from physical samples. Symbols and colour indicate sampling devices and depth as indicated in the legend.
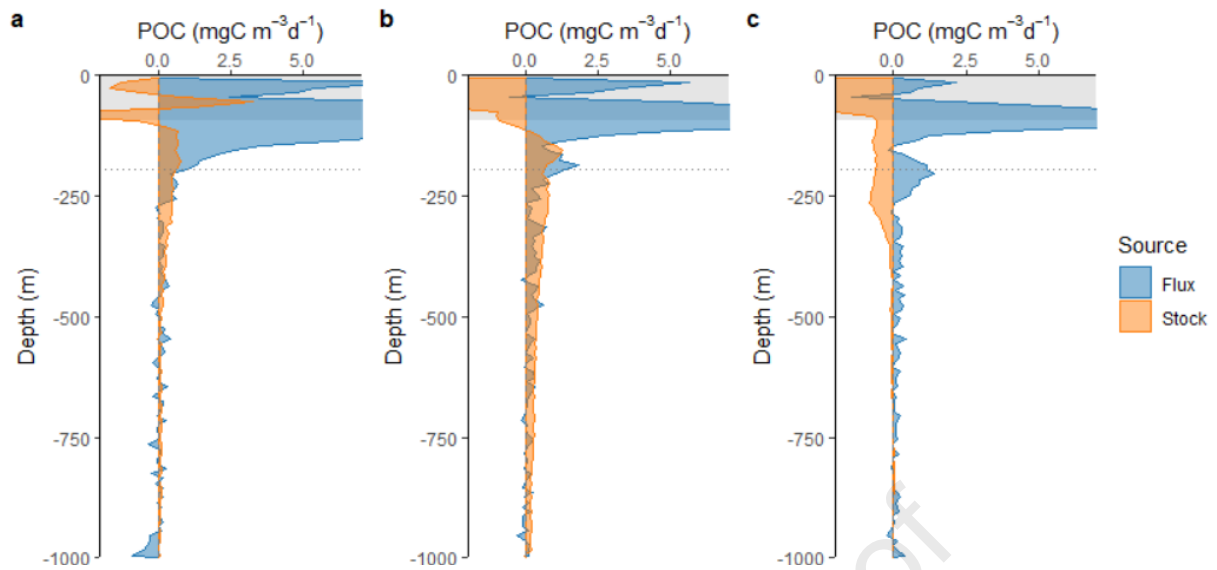
Figure S2. Mesopelagic carbon budget in high vertical resolution. Comparison of organic matter supply via sinking particles (blue) to the accumulation (or loss at P3C) of POC (orange) during the three visits (P3A, P3B and P3C). A perfect overlap of the shaded areas indicates that the accumulation of POC at that depth matches the POC supply from sinking particles. Excess orange (i.e. orange area protruding the blue-shaded area, such as in the lower mesopelagic in panel b indicates that the flux attenuation is insufficient to explain the enrichment in POC concentrations at that depth. Dashed horizontal line indicates T_{100} depth (195 m).
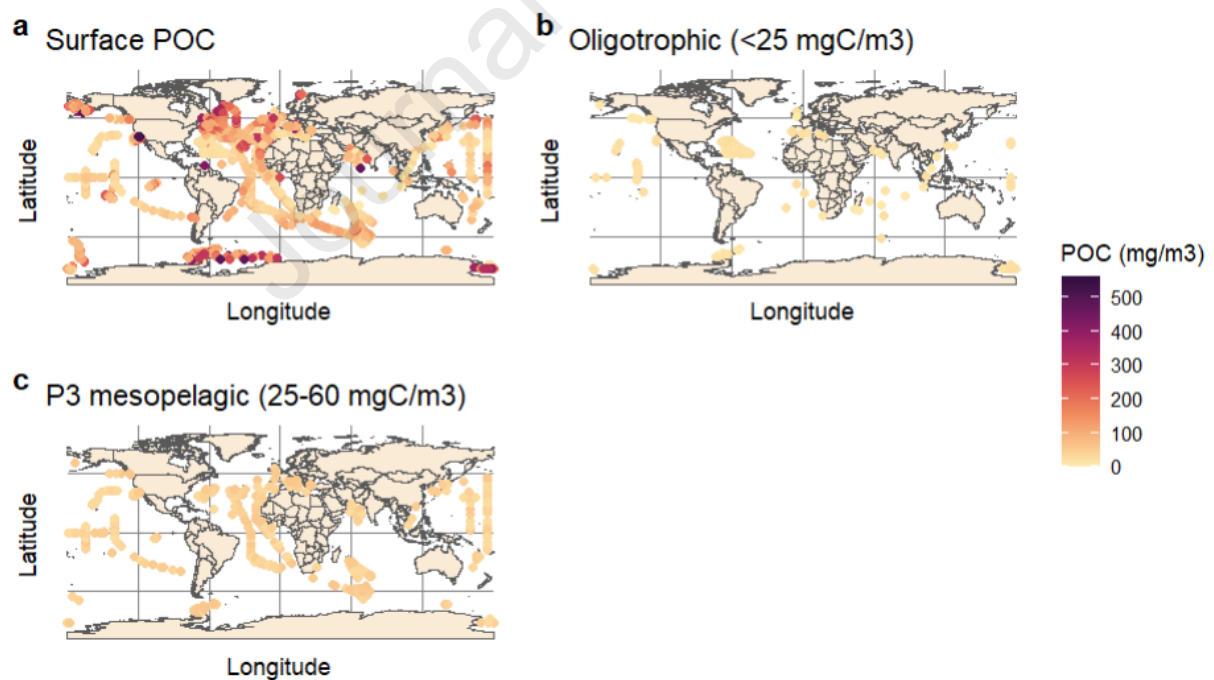
Figure S3. (a) Global database on POC concentrations in the upper 5 m (Martiny et al., 2014). (b) Only those sites where POC concentrations in the upper 5 m were lower than 20 mg C m^{-3}, indicative of oligotrophic regions. (c) Only sites where POC concentrations in the upper 5 m were between 20-60 mg C m^{-3}. 63 mgC m^{-3} is the upper concentration observed in the mesopelagic (10 m below MLD to 1000 m) during our study.

a

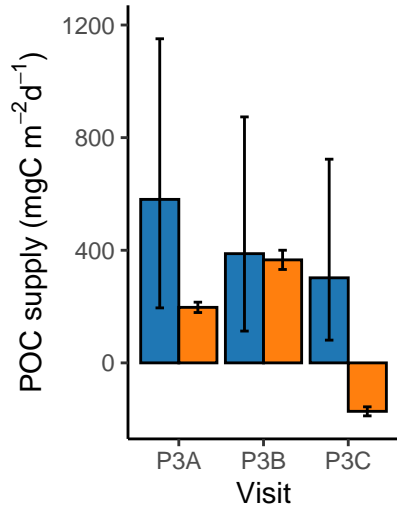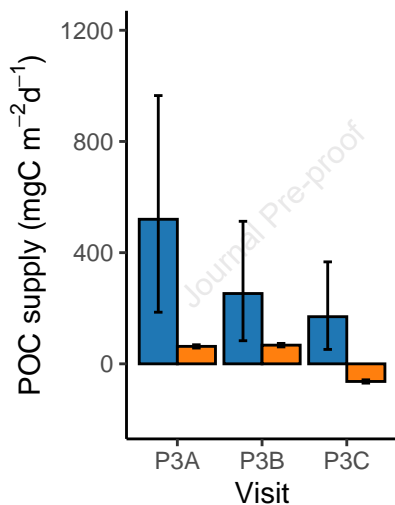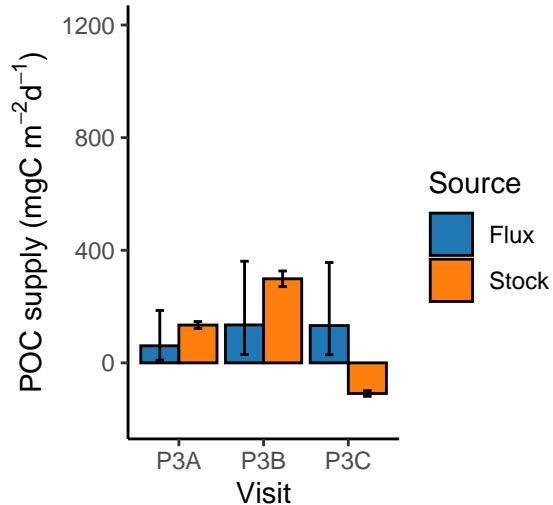Change (mg C m^{-3} d^{-1})

b

Change (d^{-1})

Depth (m)
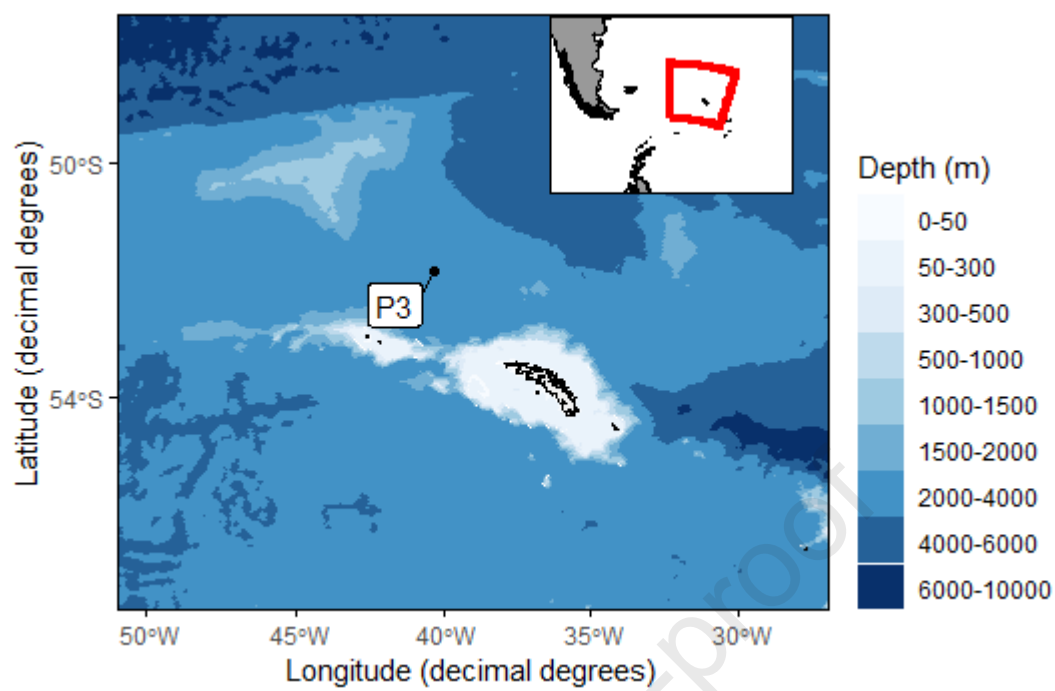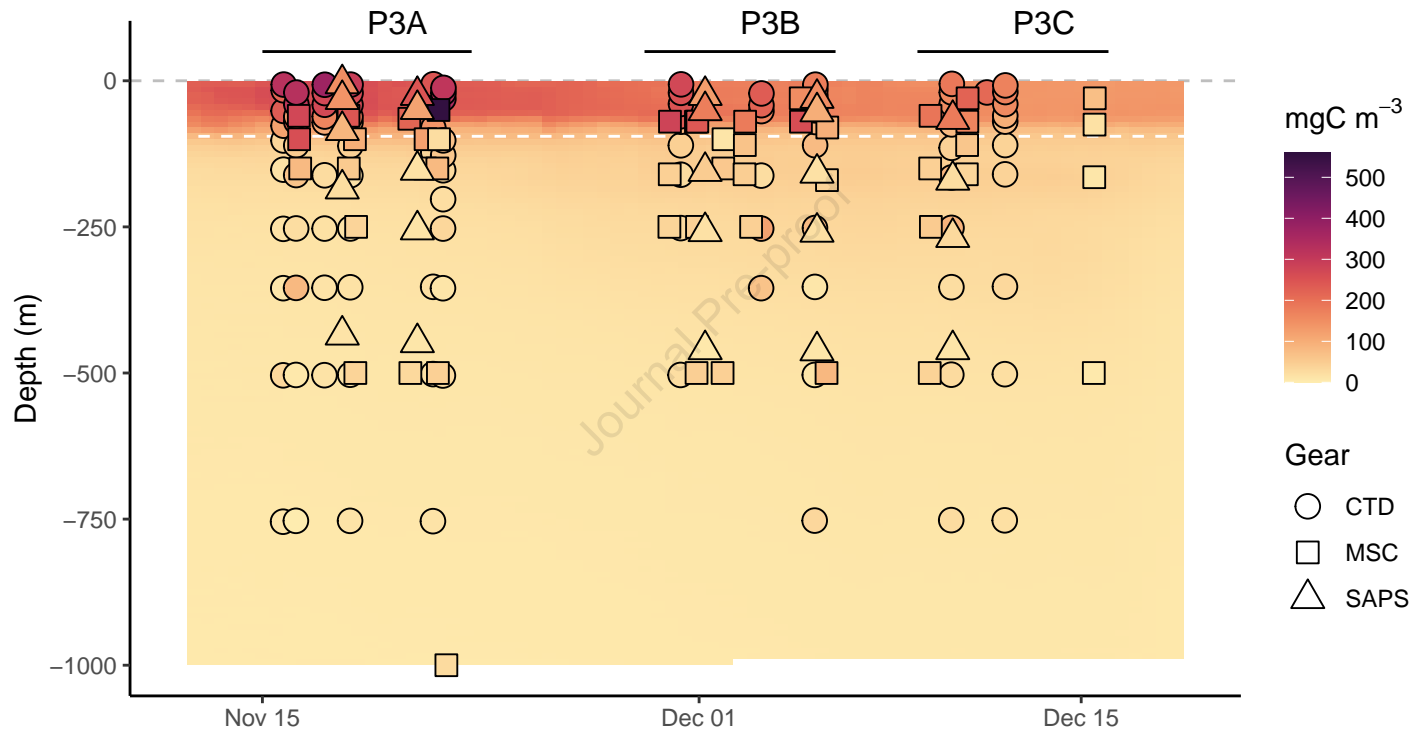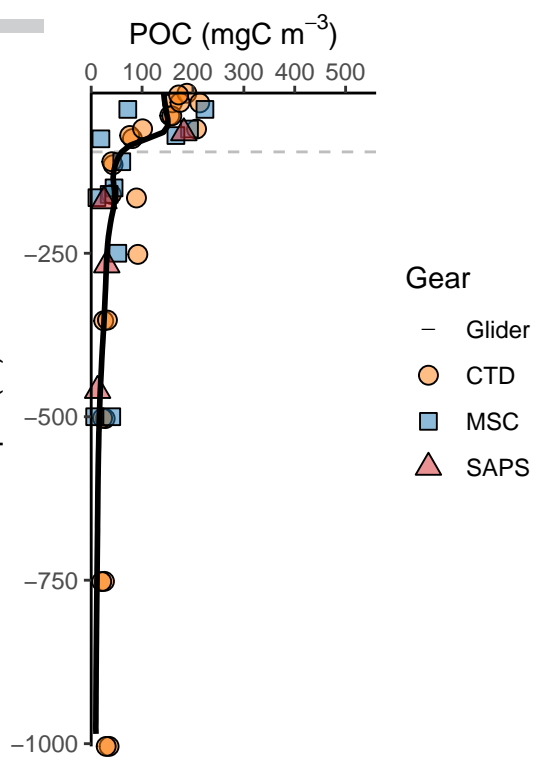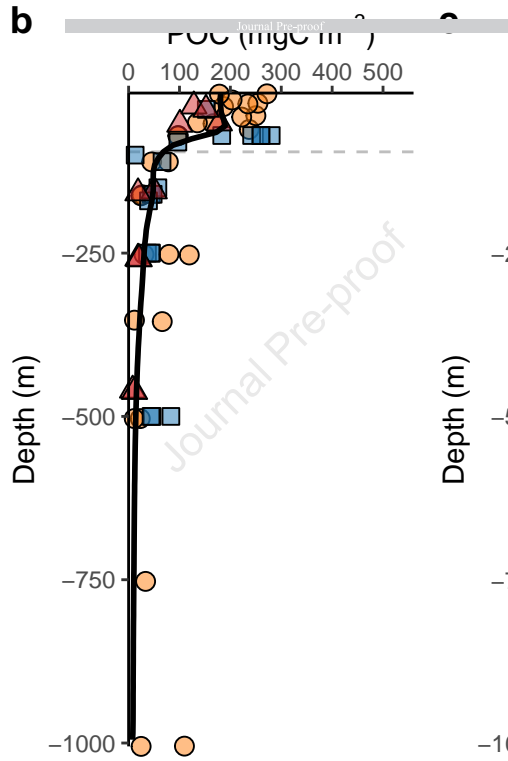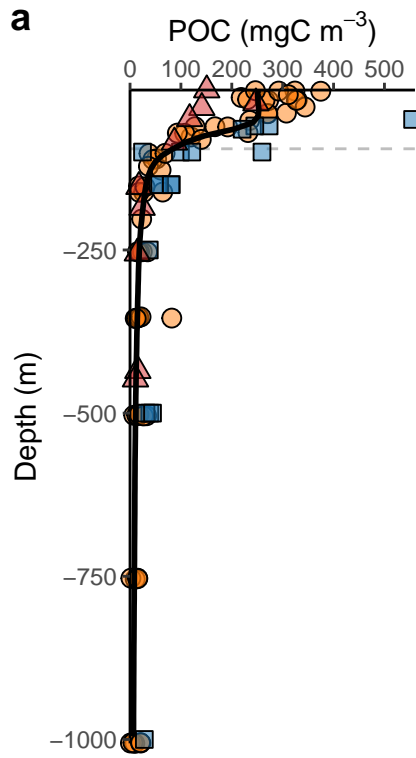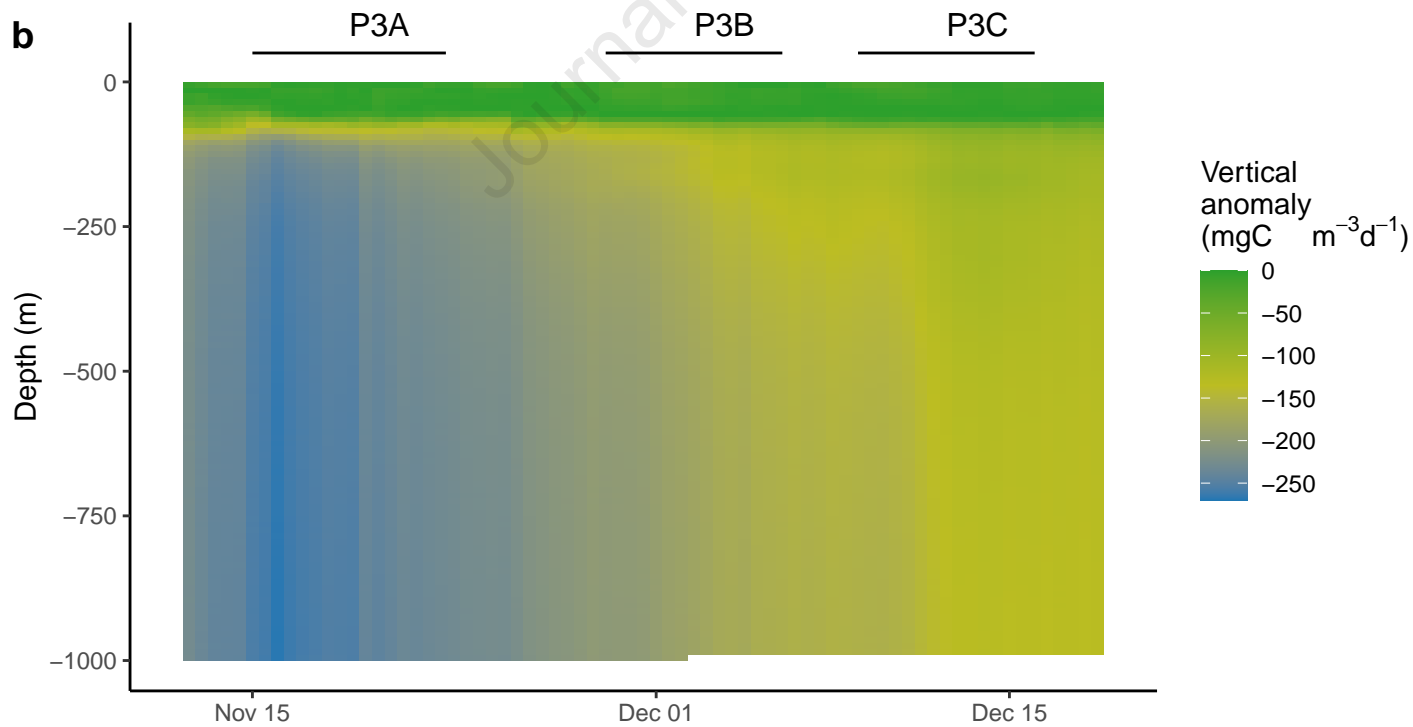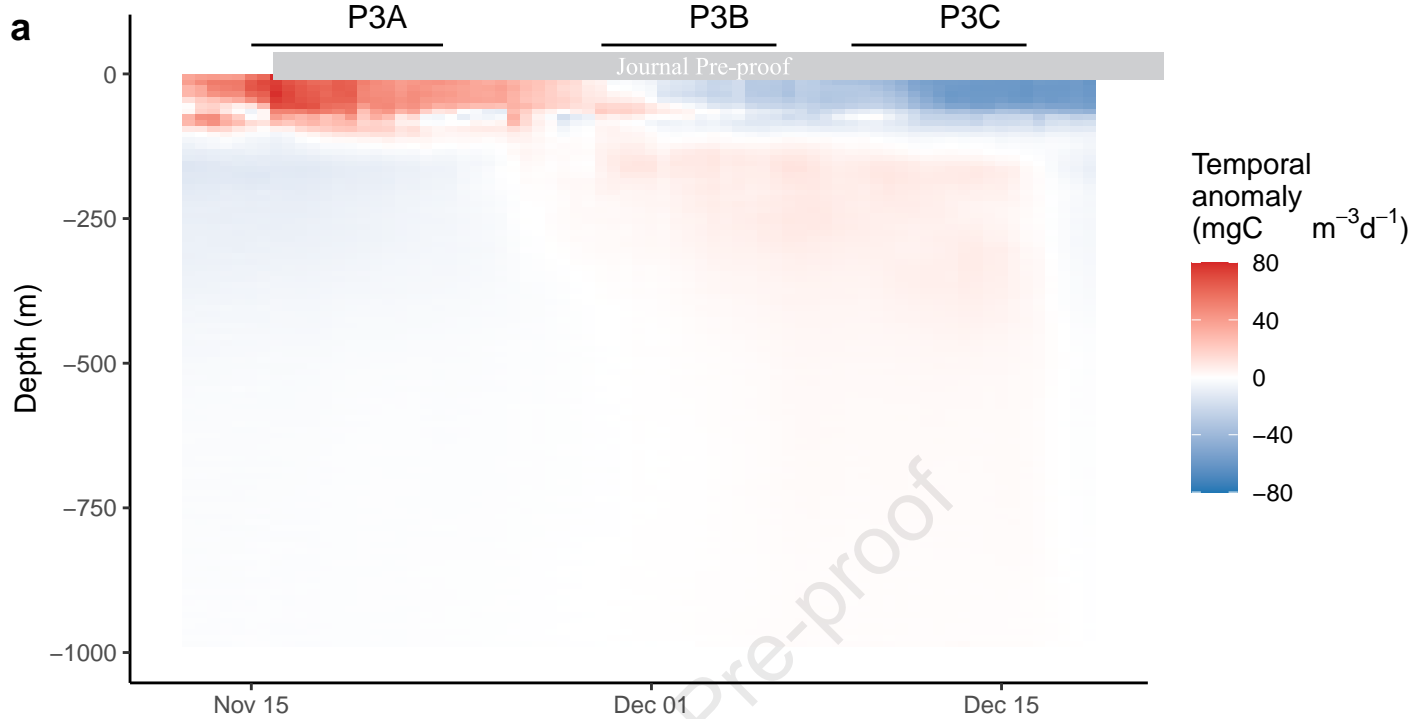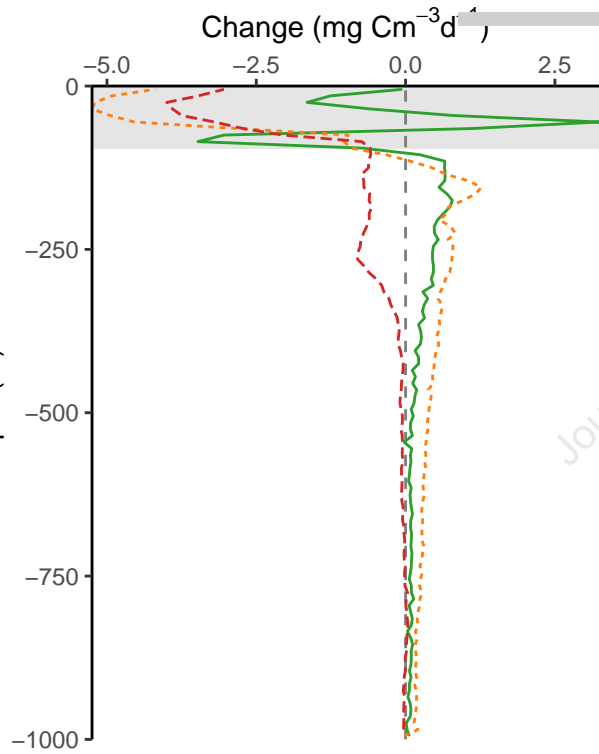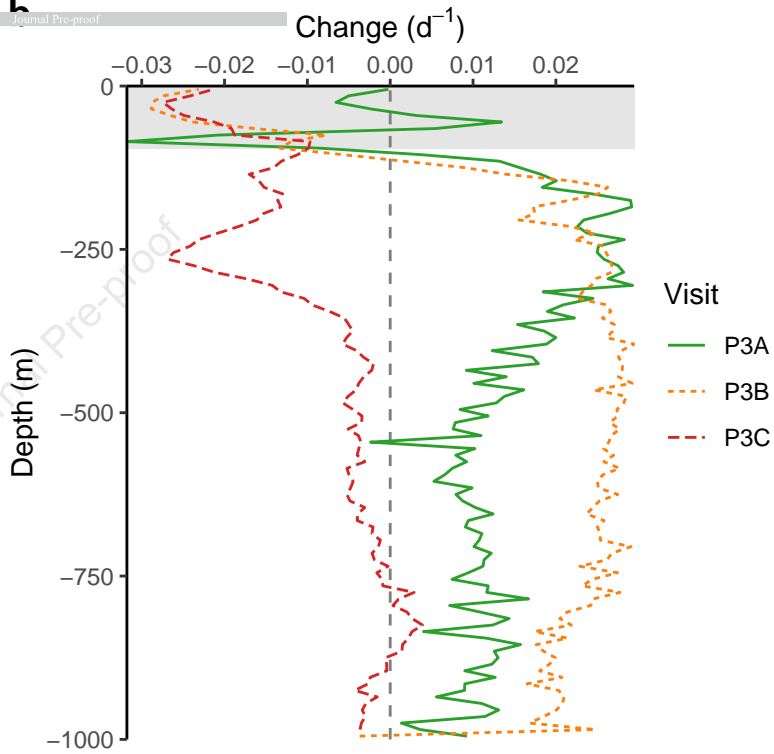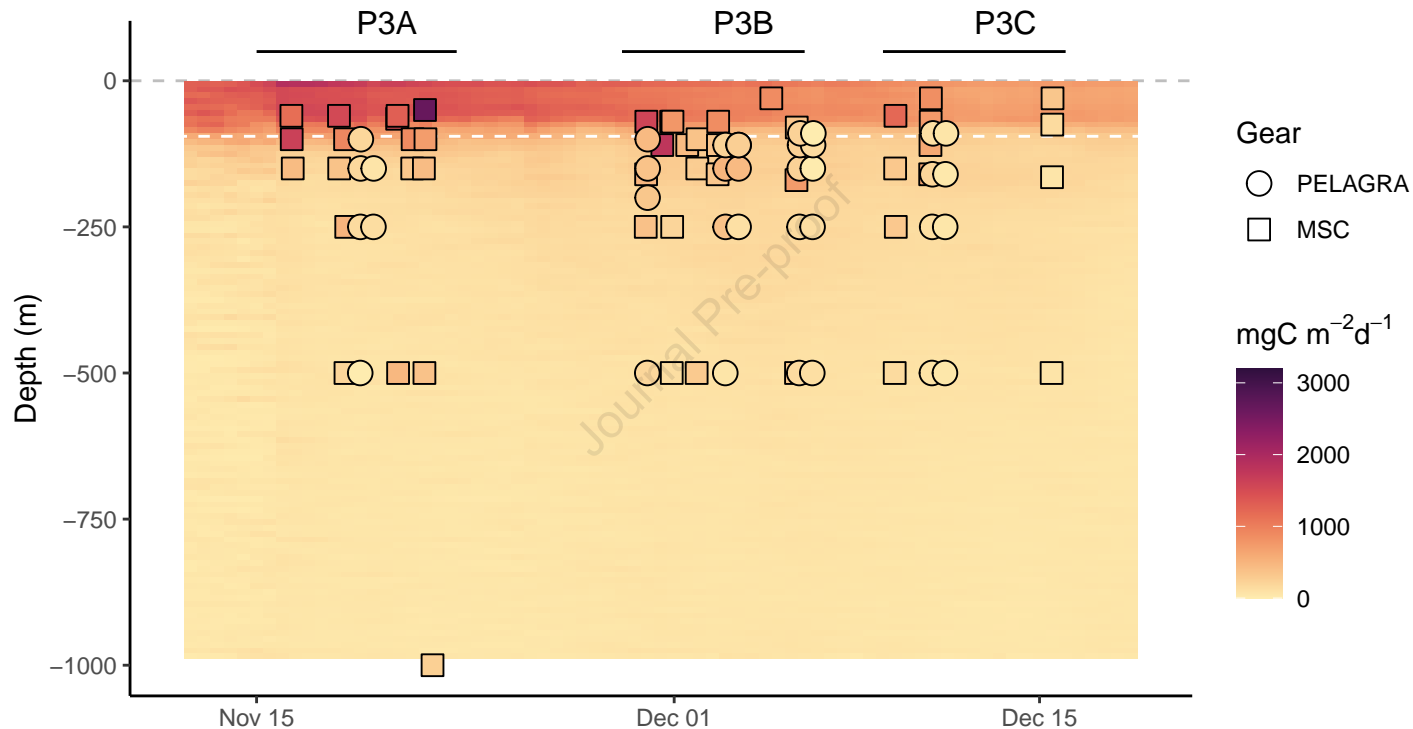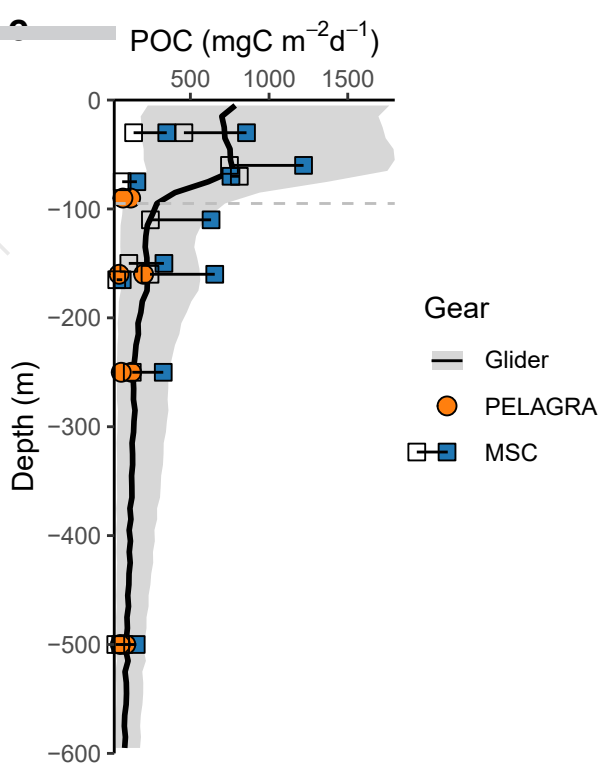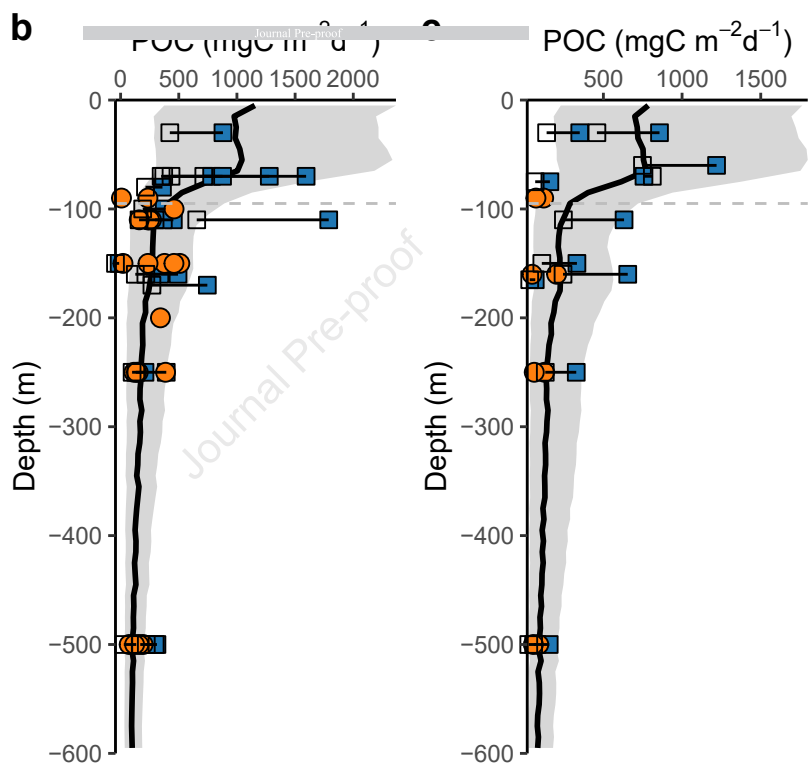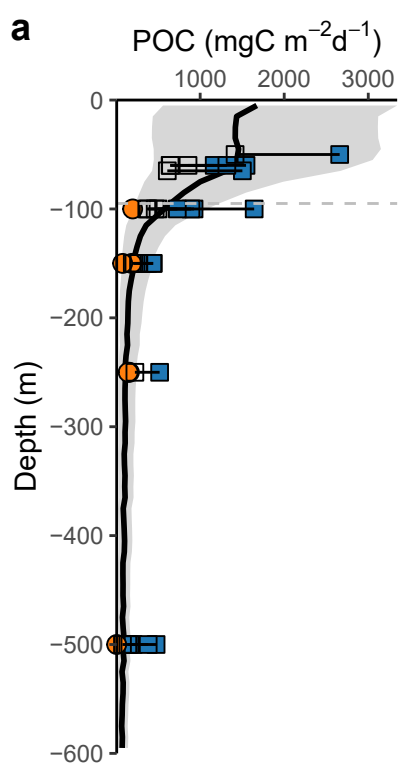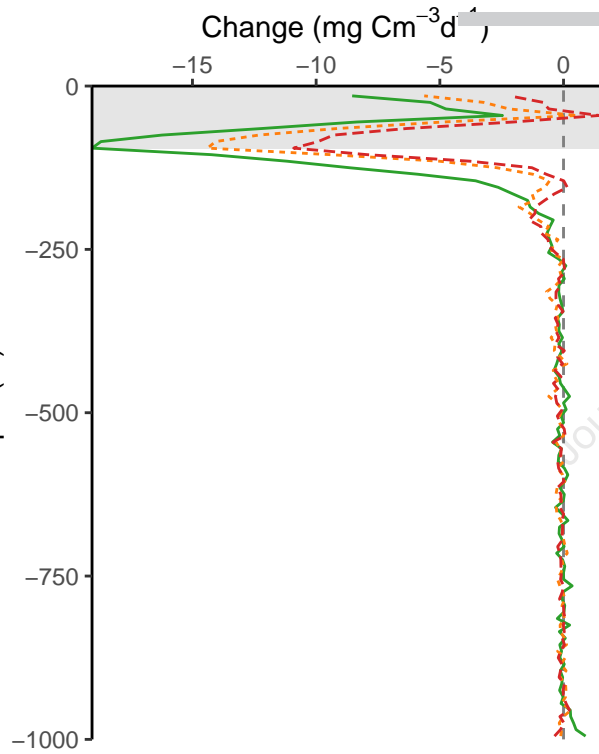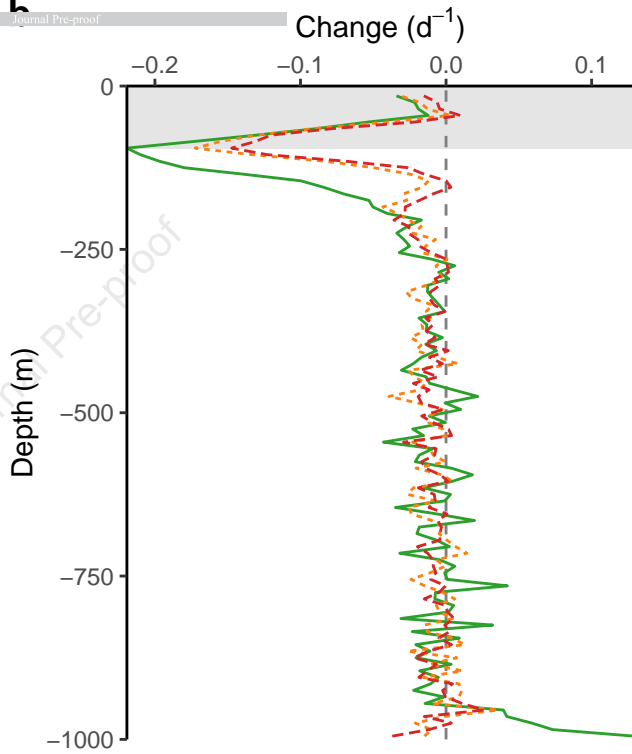
Visit

— P3A

···· P3B

– – P3C

a Total MZ: 95–1000 m **b** Upper MZ: 95–195 m **c** Lower MZ: 195–1000 m

Declaration of interests

☒ The authors declare that they have no known competing financial interests or personal relationships that could have appeared to influence the work reported in this paper.

☐ The authors declare the following financial interests/personal relationships which may be considered as potential competing interests: